The Astrophysical Journal, 647:276–292, 2006 August 10

LOW-MASS X-RAY BINARIES IN SIX ELLIPTICAL GALAXIES: CONNECTION TO GLOBULAR CLUSTERS

Eunhyeuk Kim,[1] Dong-Woo Kim,[1] Giuseppina Fabbiano,[1] Myung Gyoon Lee,[2]
Hong Soo Park,[2] Doug Geisler,[3] and Boris Dirsch[3]
Received 2005 December 2; accepted 2006 April 19

ABSTRACT

We present a systematic study of the low-mass X-ray binary (LMXB) populations of six elliptical galaxies, aimed at investigating the detected LMXB–globular cluster (GC) connection. We utilize *Chandra* archival data to identify X-ray point sources and *HST* archival data supplemented by ground observations to identify 6173 GCs. After screening and cross-matching, we associate 209 LMXBs with red GC (RGCs) and 76 LMXBs with blue GCs (BGCs), while we find no optical GC counterpart for 258 LMXBs. This is the largest GC-LMXB sample studied so far. We confirm previous reports suggesting that the fraction of GCs associated with LMXBs is ∼3 times larger in RGCs than in BGCs, indicating that metallicity is a primary factor in the GC LMXB formation. We find that GCs located near the galaxy center have a higher probability of harboring LMXBs than those in the outskirts, suggesting that there must be another parameter (in addition to metallicity) governing LMXB formation in GCs. This second parameter, dependent on the galactocentric distance, may be a distance dependent encounter rate. We find no significant differences in the shape of X-ray luminosity function, L_X/L_V distribution, X-ray spectra among RGC, BGC, and field LMXBs. The similarity of the X-ray spectra is inconsistent with the irradiation-induced stellar wind model prediction. The similarity of the X-ray luminosity functions (XLFs) of GC LMXBs and field LMXBs indicates that there is no significant difference in the fraction of black hole binaries present. We cannot either prove or reject the hypothesis that all LMXBs were formed in GCs.

Subject headings: galaxies: elliptical and lenticular, cD — galaxies: star clusters — X-rays: binaries

1. INTRODUCTION

Chandra observations of nearby early-type galaxies have shown that a large fraction (20%–70%) of low-mass X-ray binaries (LMXBs) are associated with globular clusters (GCs; e.g., Sarazin et al. 2001; Angelini et al. 2001; Kundu et al. 2002; Minniti et al. 2004; Jordan et al. 2004; see also an archival study by Sarazin et al. 2003 and a recent review by Verbunt & Lewin 2006). Moreover, a study of LMXBs near the center of NGC 4472 showed that the metal-rich red GCs (RGCs) are more likely by a factor of ∼3 to harbor LMXBs than blue GCs (BGCs; Kundu et al. 2002). This preferred association of LMXBs with metal-rich GCs (but with some variations among galaxies) was later confirmed by Sarazin et al. (2003) and Jordan et al. (2004), indicating that metal abundance plays a key role in LMXB formation; a similar trend was also known in the Milky Way (Grindlay 1993; Bellazzini et al. 1995). Several binary formation/evolution scenarios have been discussed to explain these results (e.g., Grindlay 1993; Bellazzini et al. 1995; Maccarone et al. 2004; Bildsten & Deloye 2004; Ivanova 2005); however, it is still unclear why metallicity plays such an important role in LMXB formation and what causes the observed galaxy-to-galaxy variations in the fraction of LMXBs associated with RGCs and BGCs.

The LMXB-GC association is particularly intriguing, because the high stellar density near the center of GCs may trigger the formation of binaries effectively by either three-body process or tidal capture. These binaries would then evolve into LMXBs, as first suggested by Grindlay & Hertz (1985) for the Milky Way. Given the larger density of GCs in elliptical galaxies (Harris 1991), this mechanism has been recently reproposed (Sarazin et al. 2001; White et al. 2002). The observational evidence is, however, ambiguous. The majority of LMXBs are not directly connected to GCs. The field LMXBs might have evolved from field binary stars or might have been formed in GCs and then dispersed in the field; either supernova kick or dynamical interaction within GCs have been considered as ways to extract LMXBs from their parent GC (White et al. 2002). Recently, Juett (2005) and Irwin (2005) analyzed the relation between the fraction of GC LMXBs (or their co-added X-ray luminosity of LMXBs) and the GC specific frequency (S_N) and concluded that exclusive GC formation for LMXBs may not be supported by the data. However, all these observational studies are based on relatively small GC LMXB samples, resulting from the small field of view of the *HST* observations used to identify GCs.

Here we utilize both *HST* and ground-based observations in our study of six elliptical galaxies observed with *Chandra*. Lee & Kim (2000) showed that the *HST* WFPC2 data supplemented by wide-field ground-based data are very effective for investigating GC systems of elliptical galaxies, since crowding in ground-based observations is not severe for the outer region of the galaxy. Combination of the *HST* and ground-based observations enables us not only to expand the available sample, but also to extend the study of LMXBs to the outer part of the galaxy, which has not been studied so far. It is also important to compare LMXBs and GCs in the same galaxy scale and extract their properties (e.g., the cumulative X-ray luminosity of LMXBs L_X(LMXB), the fraction of GCs associated with LMXBs f(GC LMXBs) and the GC specific frequency S_N) from the same region.

This paper is structured as follows: In § 2 we describe the sample galaxies and the data analysis method for the extraction of both LMXB and GC samples. We also explain in detail how GC candidates are selected and discuss the degree of contamination

[1] Harvard-Smithsonian Center for Astrophysics, 60 Garden Street, Cambridge, MA 02138.
[2] Department of Physics and Astronomy, Astronomy Division, Seoul National University, Seoul, 151-742, South Korea.
[3] Departamento de Fisica, Universidad de Conception, Casilla 160-C, Conception, Chile.

in the optical GC sample. The match between X-ray and optical source lists and the accuracy of astrometry are described in § 3. We report our main results in § 4. We discuss the comparisons between different LMXB populations and their implications in § 5 and summarize our main results in the last section.

2. SAMPLE SELECTION AND BASIC DATA REDUCTION TECHNIQUES

2.1. *The Sample*

We selected relatively nearby ($d \leq 30$ Mpc) elliptical galaxies with archival *Chandra* ACIS data centered on the S3 chip (Weisskopf et al. 2000) to study the characteristics of X-ray point sources. Moreover, since our goal is to investigate not only the X-ray properties of the LMXBs but also the LMXB-GC connection, we required that the sample galaxies had been observed both in optical and X-ray wavelengths. In addition, to optimize the optical coverage of our sample, we only considered galaxies where both ground-based wide-field observations and central *HST* WFPC2 pointings are available. Our final sample contains six galaxies: NGC 1399, NGC 4374, NGC 4472, NGC 4486, NGC 4636, and NGC 4649. Five of these six galaxies are in the Virgo Cluster. We list the target names along with the positions and the basic photometric properties in Table 1.

In all cases, the back-illuminated ACIS-S3 CCD was primarily used to take advantage of its higher sensitivity at the low energies ($kT < 4$ keV; *Chandra* X-Ray Center 2004). To have homogeneous X-ray data, we restricted the analysis to only data from the S3 chip even though there are still some point sources detected in the other CCDs. The observation identifier (ObsID) and exposure times of the *Chandra* observations are listed in Table 2. The effective exposure times range from 22 ks (NGC 4649) to 100 ks (NGC 4486).

Figure 1 shows the ground-based optical images of the six galaxies together with the boundaries of the *Chandra* S3 chip (*large rectangles*) and of the *HST* WFPC2 field of view (*bat-shaped regions*). The ellipses show the optical extent of the galaxy based on the standard diameter (D_{25}) and ellipticity (ϵ) from the RC3 catalog (de Vaucouleurs et al. 1991). The point sources detected in the S3 chip are marked with small circles, where the size of the circle is proportional to the size of the *Chandra* point-spread function (95% of the encircled energy fraction).

Ground-based optical observations for the six elliptical galaxies were carried out with the 4 m telescopes at Kitt Peak National Observatory (KPNO) and Cerro Tololo Inter-American Observatory (CTIO). We used the Washington *C* and standard Johnson *R* filters. The Washington filter system (e.g., *C* and T_1 filters) is known to be effective in discriminating the GCs from other contaminating sources, such as faint background galaxies and foreground stars (Geisler et al. 1996). We note that the *R* magnitude is similar to the T_1 magnitude (Kim et al. 2000; Dirsch et al. 2003), while the *R* filter has $\sim$3 times the sensitivity of the T_1 filter (Geisler 1996). We list the journal of the optical ground-based observations of the target galaxies in Table 3.

TABLE 1
List of Target Galaxies

Name	R.A.	Decl.	B_T[a]	$(m-M)_0$[b]	ϵ[a]	P.A.[a] (deg)
NGC 1399.....	03 38 29.32	−35 27 00.7	10.55	31.4	0.07	0
NGC 4374.....	12 25 03.74	+12 53 13.1	10.09	31.2	0.13	135
NGC 4472.....	12 29:46.76	+07 59:59.9	9.37	31.2	0.18	155
NGC 4486.....	12 30 49.42	+12 23 28.0	9.59	31.2	0.21	0
NGC 4636.....	12 42 50.00	+02 41 16.5	10.43	31.2	0.22	150
NGC 4649.....	12 43 40.19	+11 33 08.9	9.81	31.2	0.19	105

Note.—Units of right ascension are hours, minutes, and seconds, and units of declination are degrees, arcminutes, and arcseconds.
[a] Data from the RC3 catalog (de Vaucouleurs et al. 1991).
[b] NGC 1399 from Forte et al. (2005), other galaxies from Lee et al. (1998).

TABLE 2
Archival *Chandra* ACIS Observations

Name	ObsID	Observation Date	Exposure (ks)
NGC 1399.....	319	2000 Jan 18	56
NGC 4374.....	803	2000 Mar 19	27
NGC 4472.....	321	2000 Jun 12	34
NGC 4486.....	2707	2002 Jul 6	100
NGC 4636.....	323	2000 Jan 26	42
NGC 4649.....	785	2000 Apr 20	22

While deep ground-based optical observations provide a large enough field of view to cover the whole S3 chip, they suffer from saturation and crowding, especially in the central part of a galaxy. For these central regions, we use archival *Hubble Space Telescope* Wide Field Planetary Camera 2 (*HST* WFPC2) data. We use *V*- and *I*-band images, since these bands have been well calibrated to identify GC candidates in external galaxies (e.g., Kissler−Patig 2000). We take the F547M, F555W, and F606W filters for the *V* band and the F814W filter for the *I* band. The list of archival *HST* WFPC2 observations for the six galaxies is given in Table 4 with exposure times. The filter name for *V* band is specified when either F547M or F606W are used instead of F555W. We only list the total exposure times of multiple exposures. The mean exposure times for *V* and *I* bands of *HST* WFPC2 observation are 1950 and 1970 s, respectively.

2.2. *X-Ray and Optical Photometry*

Following the X-ray data reduction procedures in the *Chandra* Multiwavelength Project (ChaMP) (Kim et al. 2004), we clean background flare events during the exposure, then detect point sources with the CIAO task `wavdetect`. The X-ray photometric properties (count rate, hardness ratio, etc.) of point sources detected in the *B* band are computed by adding events in a circular aperture corresponding to 95% of the encircled energy of the *Chandra* point-spread function.[4]

We follow several approaches to obtain optical photometry from the ground-based observations. For NGC 4472, we use the CT_1 photometry of Geisler et al. (1996) and Lee et al. (1998). Since the *R* magnitude is very close to the T_1 magnitude (Geisler 1996), we simply consider the T_1 magnitude for point sources in NGC 4472 as their *R* magnitude. For NGC 1399, we use the wide-field photometry of Dirsch et al. (2003). For the remaining four galaxies, we use the photometric data of M. G. Lee et al. (2006, in preparation). To decrease the effect of highly varying galaxy halo light on the detection and brightness of point sources, the halo light is modeled with median smoothing at the outer radii and IRAF/STSDAS ellipse fitting tasks in the inner regions of the galaxies. Except for the very central region, where saturation truncated source detection in all ground-based observations, this modeling is very successful in reducing the effect of the galaxy light. As an example, Figure 2 shows the residual image of NGC 1399 after subtracting the model diffuse emission.

[4] See http://cxc.harvard.edu/cal/Hrma/psf.

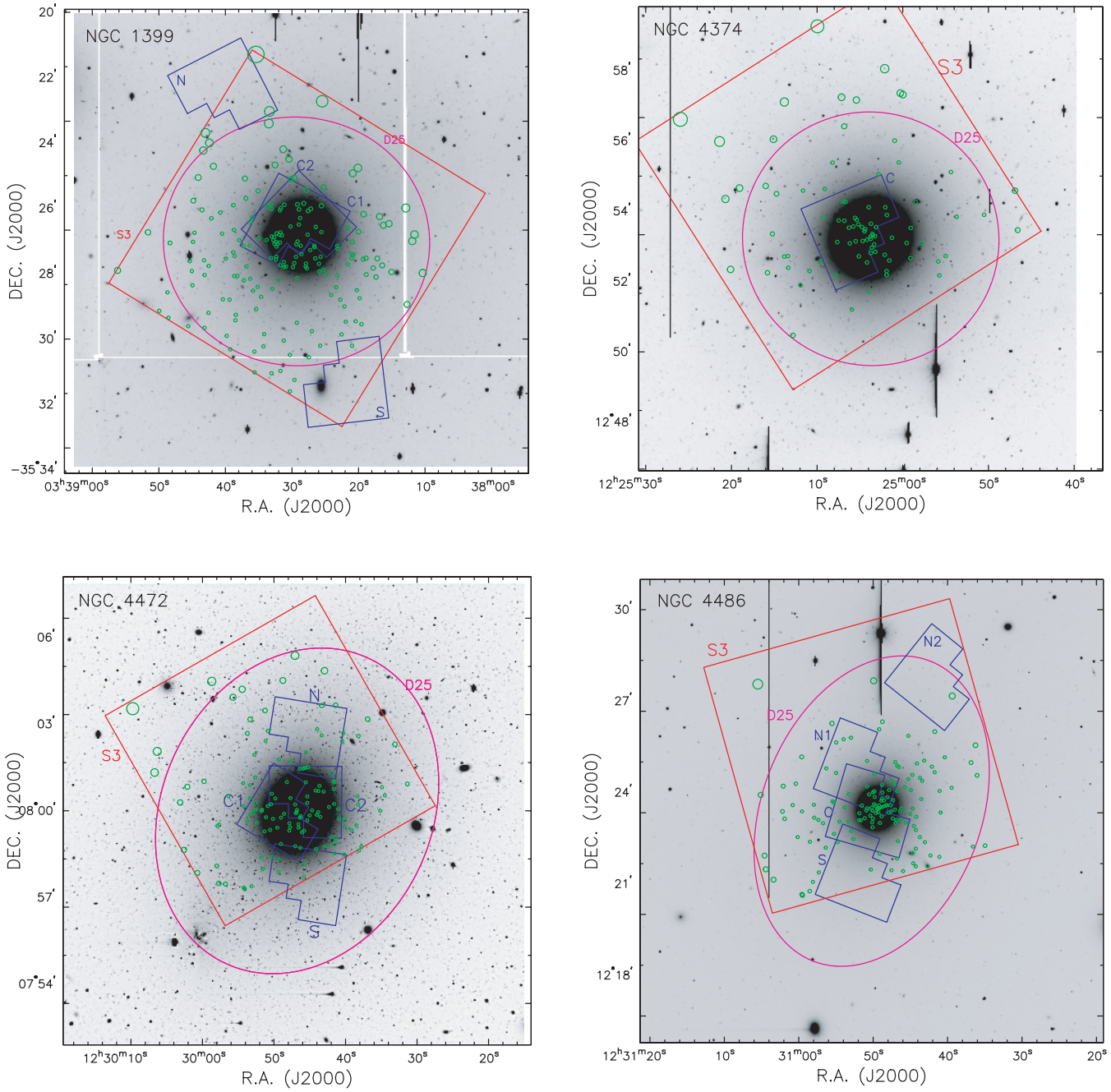

FIG. 1.—Observation fields of view for six elliptical galaxies: NGC 1399, NGC 4374, NGC 4472, NGC 4486, NGC 4636, and NGC 4649. The name of galaxy is written at the top of the each figure. The big square shows the boundary of the *Chandra* S3 chip, and the bat-shaped rectangles represent the *HST* WFPC2 fields of view with field labels (see Table 4). The optical galaxy is shown with a D_{25} ellipse. Point sources detected in S3 are shown with small circles.

We use the Lee & Kim (2000) *HST* WFPC2 photometry of NGC 4472; these authors used simple circular aperture along with appropriate aperture correction to obtain the photometry of point sources. For the remaining five galaxies, we perform our own *HST* WFPC2 photometry in this study. Images obtained with the same filter are combined if there are multiple images, to remove cosmic-ray hits. Rejection of cosmic rays is important, especially for the *HST* WFPC2 observation. Because the *HST* point-spread function is comparable to the size of cosmic-ray hits, a cosmic ray is more likely misidentified as a valid point source in the *HST* observations than in ground-based observations. To remove the galaxy diffuse emission, we apply the same modeling technique as used for the ground-based observations. For the final photometry, we utilize the digital photometry software HSTPHOT (Dolphin 2000; Kim et al. 2002).

For the four galaxies NGC 4374, NGC 4486, NGC 4636, and NGC 4649, we obtain surface photometry of images from ground-based observations using the `ellipse` task of IRAF/STSDAS. Iteratively fitting an ellipse to isodensity contours (Jedrzejewski 1987), `ellipse` provides radial profiles of brightness, color, ellipticity, and position angle. The ellipse fitting results are shown in Figure 3. For comparison, we also plot the NGC 4472 (Kim et al. 2000; *solid lines*) and NGC 1399 (Dirsch et al. 2003; *dashed lines*). Based on the *R*-band surface photometry, we list in Table 5 the basic structure parameters, including effective radius ($R_{\rm eff}$) and standard radius (R_{25}), a circular radius of an ellipse where the

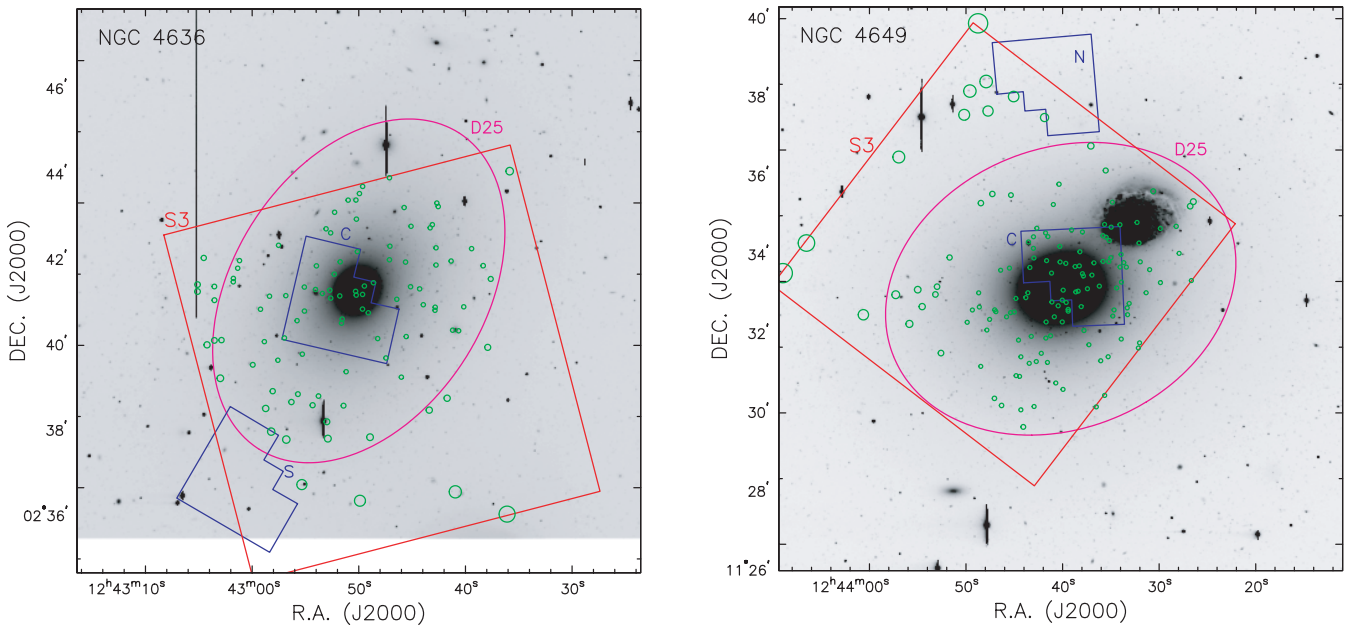

FIG. 1.—*Continued*

surface brightness in B band is $\mu_B = 25$. Also listed are ellipticities, position angles, and colors at these two radii. We measure the mean color and magnitude and color gradient in the region of $R_{\rm eff} \leq R \leq R_{25}$ (the last three rows in Table 5). We note that the mean optical properties are similar in different galaxies, with the possible exception of NGC 4636, which has a slightly bluer color in the outer radii.

2.3. *Optical Globular Cluster Candidates*

Multicolor observations are frequently used for selecting GC candidates, since GCs show a typical distribution in a color magnitude diagram (CMD), especially in the $(V - I) - V$ and $(C - R) - R$ domains (Geisler et al. 1996; Lee & Kim 2000). Figure 4 shows the distribution of optical point sources in the $(V - I) - V$ CMD for *HST* WFPC2 observations and in the $(C - R) - R$ CMD for the ground-based observations of the six elliptical galaxies. The boxes represent the selection criteria for GC candidates adopted in the present study. Since most of the sample galaxies are in Virgo, we used the same magnitude boundaries defined by Geisler et al. (1996) for ground-based observations ($19.65 < R < 23.5$) and by Lee & Kim (2000) for the *HST* WFPC2 observations ($V < 23.9$). However, we applied slightly different color boundaries (by not more than ~0.1 mag) from one galaxy to another to optimize the GC selection and to take into account galaxy-to-galaxy variations, such as internal extinction and mean metallicities. The adopted color boundaries are listed in Table 6. Our results do not change if we apply a single color boundary, (that of NGC 4472) in all galaxies. On average, the fraction of BGCs and RGCs hosting LMXBs changes by ~6%.

Since point sources detected in *HST* WFPC2 observation are less likely confused than those from ground-based observations, we preferentially use *HST* WFPC2 data whenever possible. *CR* photometries are transformed to *VI* photometries by using point sources detected in both *HST* WFPC2 and ground-based observations. The total number of GC candidates in the six galaxies is 6173 in a radial region of $20'' < R < R_{25}$. M87 (NGC 4486) is

TABLE 3
JOURNAL OF OPTICAL GROUND-BASED OBSERVATIONS

Name	Observation Date	Telescope	Filters	References
NGC 1399.....	1999 Dec 7	CTIO 4 m	*CR*	1
NGC 4374.....	1997 Apr 8	KPNO 4 m	*CR*	2
NGC 4472.....	1993 Feb 26	KPNO 4 m	CT_1	3, 4
NGC 4486.....	1997 Apr 9	KPNO 4 m	*CR*	2
NGC 4636.....	1997 Apr 10	KPNO 4 m	*CR*	2
NGC 4649.....	1997 Apr 9	KPNO 4 m	*CR*	2

REFERENCES.—(1) Dirsch et al. 2003; (2) M. G. Lee et al. 2006, in preparation; (3) Geisler et al. 1996; (4) Lee et al. (1998).

TABLE 4
JOURNAL OF *HST* WFPC2 OBSERVATIONS

Name	Field	$T_{\rm exp}$ (s) V[a]	$T_{\rm exp}$ (s) I[b]	Program ID
NGC 1399.....	C1	...	1800	5990
	C2	4000 (F606W)	...	8214
	N	3500 (F606W)	900	9244
	S	460	300	6352
NGC 4374.....	C	280 (F547M)	520	6094
NGC 4472.....	C1	1800	1800	5236
	C2	520	520	5236
	N	2200	2300	5920
	S	2200	2300	5920
NGC 4486.....	C	2430	2430	5477
	N1	2000	1800	6844
	N2	400	800	7274
	S	2000	1800	6844
NGC 4636.....	C	1000 (F547M)	400	8686
	S	1800	1820	8686
NGC 4649.....	C	2100	2500	6286
	N	4800	9600	7388

[a] F555W if not mentioned.
[b] F814W.

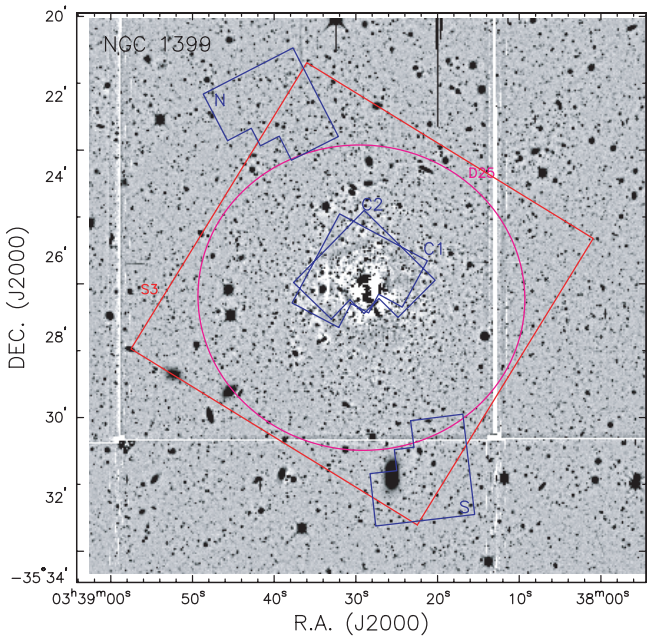

FIG. 2.—Ground-based *C* filter image of NGC 1399. Galaxy halo light is removed using ellipse fitting and the median filtering method (see text).

found to have the most populous GC system ($N_{GC} = 1906$), while NGC 4374 has only 523 GCs. In Table 7 we summarize the number of GCs found in ground and *HST* observations.

To illustrate how the contamination fraction varies as a function of the optical magnitude and color, in Figure 5 we place various CMD regions in the same sense as in each CMD of Figure 4, i.e., horizontally along the optical color ($C - R$) and vertically along the optical magnitude (R). The fraction of point sources detected only in ground-based observations (but rejected as extended sources in *HST* WFPC2 observations) and point sources detected in both ground-based and *HST* WFPC2 observations are marked by triangles and filled circles in Figure 5, respectively. Although the degree of contamination varies slightly from one galaxy to another, the global amount of contaminants for the sample of GC candidates in ground-based observations is ~14% for CMD regions BGC and RGC. The contamination increases dramatically when we consider the fainter samples (CMD regions FB and FR in Fig. 5) or sources with extreme colors (CMD regions VB and VR in Fig. 5).

Even with the above selection criteria, a nonnegligible fraction of interlopers remain in the selected GC candidates, since there are some background galaxies that have magnitudes and colors located in the selection boxes of the CMDs in Figure 4.

We first estimate the number of these contaminants detected in the *HST* WFPC2 observation by utilizing archival observations of the blank sky (six pointings at 40′–60′ away from the center of M87), where no GC associated with M87 is expected. Applying the same photometric technique to these *HST* WFPC2 observations as we used on our data, we find on average of ~0.5 sources arcmin^{-2} located in the same CMD region of our GC candidates. Our estimate is a factor of ~2 lower than 1.2 sources arcmin^{-2} measured from Figure 3 in Larsen et al. (2001). We note that this number (0.5) will increase by a factor of ~4 for fainter sources ($V < 25$ mag), showing a good agreement with the background estimation of Kundu et al. (1999). Conservatively, we take the higher contamination fraction (1.2 sources arcmin^{-2}), which corresponds to ~2% of the GC sample detected in the *HST* WFPC2 observations of the six galaxies.

We then estimate the number of contaminants detected in the ground observations by comparing the number of ground detection with that of *HST* WFPC2 detection in the same field.

This estimate depends not only on the observational status (e.g., exposure time, filter system), but also on the distribution of sources within the galaxy. Based on simulations, Lee & Kim (2000) showed that in the inner region of NGC 4472, the incompleteness due to the highly varying galaxy light and source crowding is negligible only when bright ($V \leq 24$ mag) sources outside the crowded center ($r \geq 10''$) are used.

The contamination fraction increases with the galactocentric distance because the GC population decreases with increasing distance while the number of background sources remains constant. We show the radial variation of the fraction of GCs detected only in the ground data in Figure 6. The line represents the best fit assuming a power-law distribution for GCs and a uniform distribution for background sources. While the contamination fraction is small near the center (e.g., <10% for $R < R_{eff}$), it can be as high as ~20% at $R = R_{25}$. We correct for the radius-dependent contamination throughout this paper (e.g., Table 11).

Applying this contamination fraction to the GC candidates selected from ground observations alone, we estimate the number of contaminants in BGC and RGC candidates of ground-based observation at different galactocentric radii and list the numbers in the last two columns of Table 7. The total number of background galaxies that might be included in the current optical globular cluster sample ($20'' \leq R \leq R_{25}$) is ~9%. The contamination increases with galactocentric radii due to the lack of *HST* WFPC2 observations in the outer part of a galaxy. The fraction of contaminants for the inner regions (outside the central 20″) is less than 5%, while this value increase to ~12% for the region outside the D_{25} ellipse.

As an independent test to address the contamination in the sample of ground-based observations, we utilize the source catalogs from Hubble Deep Fields north and south (Williams et al. 1996; Casertano et al. 2000). Since the typical seeing size of ground-based observations is ~1″, we only consider extended sources with a size smaller than 1″, which might be misclassified as a point source in ground-based observations. Counting the number of HDF sources located in the same CMD region with our optical GCs, we find that the misclassified extended galaxies could be ~13% of our ground-based optical GC sample, corresponding to ~8.4% of our GC sample. We conclude that the effect of contamination in our GC sample is small (<10%).

3. MATCHING X-RAY AND OPTICAL POSITIONS

3.1. *Astrometric Uncertainty*

To accurately determine the X-ray source position, we first corrected for the aspect offset introduced by the earlier inaccurate calibration data (see CIAO science thread[5]). After running `wavdetect`, we also applied a position refinement algorithm (Kim et al. 2004), which was later incorporated into CIAO version 3.0 `wavdetect`.[6] The X-ray source positional error is then calculated by the prescription given by Kim et al. (2006), who provide a set of empirical equations as a function of source count and off-axis angle, based on extensive simulations. The positional uncertainty of a typical X-ray source with 30 net counts at off-axis angle 4′ is 0.″83 at the 95% confidence level.

The optical source position in pixel coordinates is determined by `daophot` (Stetson 1987) for ground-based observations and

[5] See http://asc.harvard.edu/ciao/threads/arcsec_correction.
[6] See http://cxc.harvard.edu/ciao.

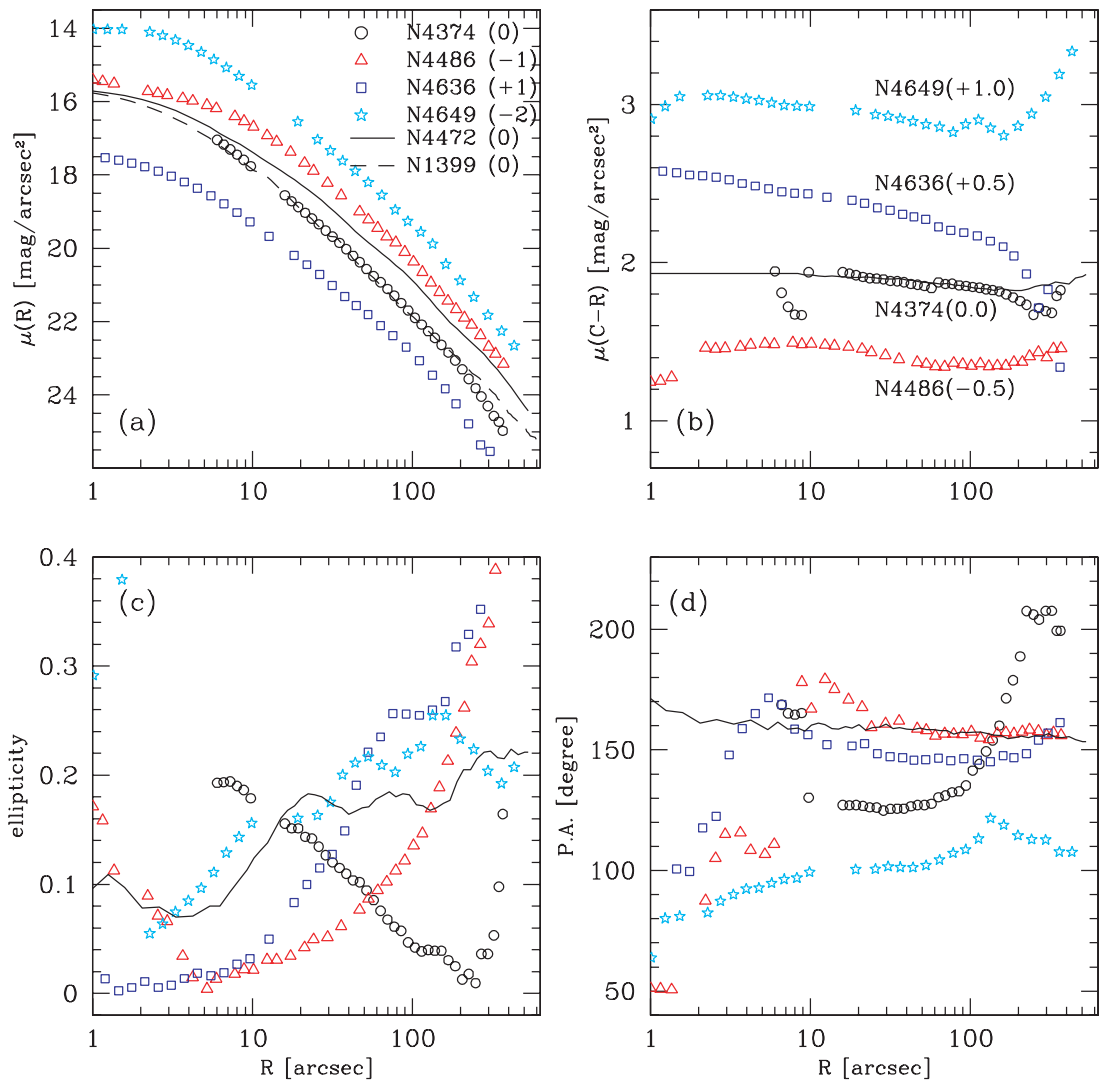

FIG. 3.—Surface photometry of four elliptical galaxies: radial profiles of (*a*) *R*-band surface brightness, (*b*) $(C - R)$ surface color, (*c*) ellipticity in the *R*-band image, and (*d*) position angle in the *R*--band image. NGC 4472 (Kim et al. 2000) and NGC 1399 (Dirsch et al. 2003) are also shown for comparison with solid and dashed lines, respectively.

TABLE 5

STRUCTURAL PARAMETERS OF THE STUDIED ELLIPTICAL GALAXIES

Parameter	NGC 4374	NGC 4486	NGC 4636	NGC 4649	NGC 4472[a]	NGC 1399[b]
$R_{\rm eff}$ (arcmin)	1.20	1.53	1.49	1.50	2.00	2.50
$\epsilon_{\rm eff}$	0.065	0.125	0.256	0.216	0.175	0.099
P.A.$_{\rm eff}$ (deg)	67	159	148	112	155	...
$(C - R)_{\rm eff}$	1.87	1.86	1.69	1.88	1.83	...
R_{25} (arcmin)	3.63	4.36	3.60	4.03	5.22	3.93
ϵ_{25}	0.016	0.320	0.326	0.224	0.200	0.17
P.A.$_{25}$ (deg)	67	159	148	112	155	...
$(C - R)_{25}$	1.74	1.93	1.45	1.92	1.88	...
$\langle C - R \rangle$[c]	1.81	1.88	1.57	1.85	...	...
$\Delta\mu(R)/\Delta \log R = 1$[c]	4.64	4.60	5.20	5.13	...	
$\Delta(C - R)/\Delta \log R = 1$[c]	−0.232	0.219	−0.612	0.036	−0.08	...

[a] Kim et al. (2000).
[b] Dirsch et al. (2003).
[c] Values computed between effective radius and standard radius.

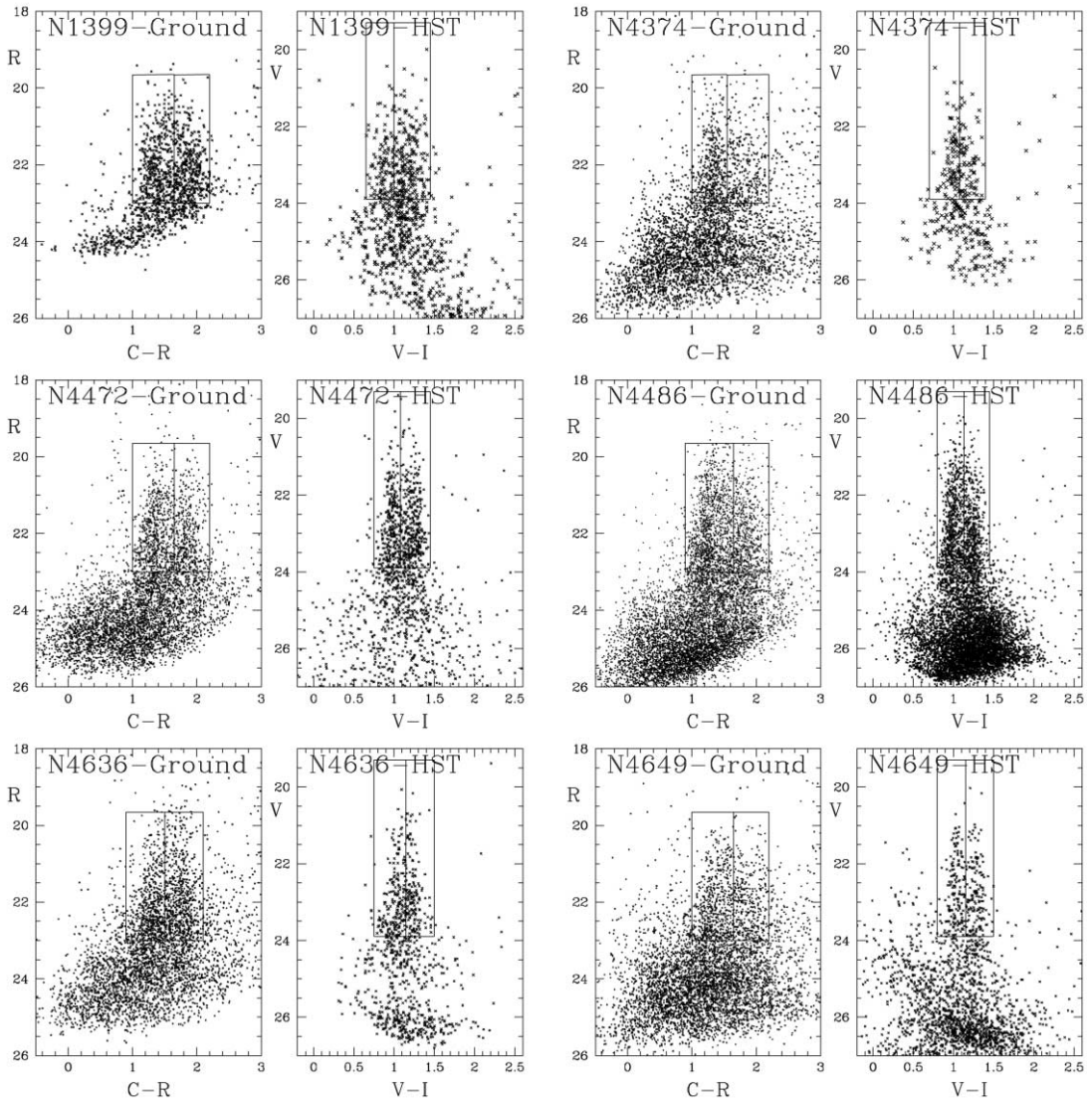

FIG. 4.—CMDs of point sources detected in ground and *HST* WFPC2 observations. The selection boundaries of GC candidates are shown with rectangles (see text).

HSTPHOT (Dolphin 2000) for *HST* WFPC2 observations, respectively. The pixel coordinate is then transformed to the world coordinate by cross-correlating the USNOB1 catalog (Monet et al. 2003). A typical error of this transformation is $\sim 0\farcs3$. However, we cannot use the USNOB1 catalog for the *HST* WFPC2 data because there are only a small number of USNOB1 sources inside the *HST* WFPC2 field of view, particularly when it is aiming at the center of a galaxy, which is often saturated and also highly nonuniform. Instead, we use the transformed ground-based data as a template to obtain the world coordinate for *HST* WFPC2 sources. The transformation error between the ground-based data and *HST* WFPC2 data is dominated by the former error ($\sim 0\farcs3$) due to the negligible positional error of the *HST* WFPC2 data.

TABLE 6
ADOPTED COLOR BOUNDARIES OF GCs

	$C-R$		$V-I$	
NAME	BGCs	RGCs	BGCs	RGCs
NGC 1399.....	1.00–1.65	1.65–2.20	0.65–1.00	1.00–1.45
NGC 4374.....	1.00–1.55	1.55–2.20	0.70–1.08	1.08–1.40
NGC 4472.....	1.00–1.65	1.65–2.20	0.75–1.08	1.08–1.45
NGC 4486.....	0.90–1.65	1.65–2.20	0.80–1.13	1.13–1.45
NGC 4636.....	0.90–1.50	1.50–2.10	0.75–1.15	1.15–1.50
NGC 4649.....	1.00–1.65	1.65–2.20	0.80–1.15	1.15–1.50

3.2. *Match and Random Match*

Using the X-ray positional errors at the 95% confidence level (Kim et al. 2006), we first select optical sources inside the *Chandra* error radius. To minimize false matches, we further limit the search radius to $1\farcs2$ and visually inspect the optical image for validation. Most (>91%) X-ray sources have error radii smaller than $1\farcs2$. When there are multiple optical sources inside the search radius, we select the nearest optical source. Since this happens only 11 times (or for a few percent of the sources), the expected number of false matches is negligible. For 85% of the matches, the positional offset between X-ray and optical sources ($d_{\rm xo}$) is less than the typical positional error of X-ray sources ($0\farcs83$). The median positional offset is $d_{\rm xo} = 0\farcs5$.

To identify field LMXBs (i.e., X-ray sources without an optical counterpart), we first select the X-ray sources without optical counterpart inside $d_{\rm xo} = 1\farcs2$. We then visually inspect the optical images at the position of X-ray sources to look for optical

TABLE 7
Optical GCs

Name	BGCs		RGCs		Contamination	
	G[a]	H[2b]	G[a]	H[b]	BGCs	RGCs
$20'' \leq R < R_{\rm eff}$						
NGC 1399.....	134	72	153	148	16	18
NGC 4374.....	20	48	21	42	2	2
NGC 4472.....	33	178	32	244	3	3
NGC 4486.....	87	245	72	278	9	7
NGC 4636.....	46	123	65	95	5	7
NGC 4649.....	38	102	43	121	4	4
Total	358	768	386	928	39	41
$R_{\rm eff} \leq R < R_{25}$						
NGC 1399.....	154	5	129	4	30	25
NGC 4374.....	207	23	142	20	35	24
NGC 4472.....	341	58	194	53	60	34
NGC 4486.....	680	154	287	103	116	49
NGC 4636.....	265	19	299	13	47	53
NGC 4649.....	331	39	203	10	58	35
Total	1978	298	1254	203	346	220
$R_{25} \leq R$						
NGC 1399.....	75	19	45	21	18	11
NGC 4374.....	173	0	106	0	42	26
NGC 4472.....	73	0	40	0	18	10
NGC 4486.....	113	42	17	14	28	4
NGC 4636.....	171	15	148	13	42	36
NGC 4649.....	147	6	72	6	36	18
Total	752	82	428	54	184	105

[a] Number of sources in optical ground observation only regions.
[b] Number of sources in *HST* observation regions.

counterparts just outside the error circle and undetected sources due to chip defects and/or saturation effect of nearby bright sources. In our sample of 665 X-ray point sources inside the D_{25} ellipse (but excluding the central $20''$ region), we identify 285 (43%) GC LMXBs and 258 (39%) field LMXBs. We list the match statistics for each galaxy in Table 8. Since our match criteria are rather conservative, we are left with 122 X-ray sources for which we cannot establish whether they match with GCs or not. Some of them match with non-GC optical sources. We do not use these X-ray sources in the following analysis to minimize the uncertainty of X-ray source characteristics.

To assess the probability of false matches, we applied two independent methods. First, to determine the probability of finding an optical source by chance, we shifted the X-ray source position by $5''$, corresponding to $\sim$6 times the typical 95% position error, and then we tried to match them with optical sources as explained above. Based on 100 simulations for the whole S3 field of view, we find $\sim 17 \pm 1$ ($\sim$2.5%) matches, which is considerably smaller than the 43% match occurrence obtained for the observed X-ray source positions. Second, we redistributed the optical sources randomly, but following the observed GC radial profile, and kept the number of sources the same as that of the observed sources. The number of random matches with optical GCs is $N = 34 \pm 4$ (or $\sim$5%), and decreases (by $\sim$30%) when X-ray sources in $r < 20''$ are excluded. Adopting the radial profile of the halo light instead of the GC profile affects very little the number of random matches ($N = 41$). Therefore, we conclude that the chance probability of a false match is small compared to the number of GC-LMXB associations.

We summarize the match statistics for the point sources in this radial range in Table 9. The mean probability for a GC to harbor an LMXB, defined by $f_{\rm GC} = N({\rm GC\text{-}LMXB})/N({\rm GC})$, is $\sim$5.2% in our sample of six galaxies, or $\sim$4.4% in Virgo galaxies only. This is somewhat larger than that for the central region of NGC 4472 (Kundu et al. 2002) and NGC 1399 (Angelini et al. 2001). The main difference is due to different color-magnitude criteria. Kundu et al. (2002) selected GCs with $V < 26.5$ mag and Angelini et al. (2001) with $B < 28$ mag. However, we note that adding more faint GC candidates does not add many reliable GC-LMXB associations. As an example, there is only one faint GC hosting an LMXB with $V > 24$ mag in the combined sample of the two previous studies. On the other hand, the contamination fraction considerably increases with decreasing optical brightness (see § 2.3). To estimate the effect of the difference in distance between NGC 1399 and the Virgo ellipticals, we recalculate $f_{\rm GC}$ for NGC 1399 by changing the magnitude limit by 0.2 mag: $f_{\rm GC}$ decreases only by 0.7%.

While the fraction of BGCs with an LMXB ($f_{\rm BGC}$) is relatively constant ($\sim$2%) with the exception of NGC 1399 (5.8%), that of RGCs ($f_{\rm RGC}$) varies widely from one galaxy to another (2.7%–13%), resulting in $f_{\rm RGC}/f_{\rm BGC}$ varying from 1.4 to 4.6. The average $f_{\rm RGC}/f_{\rm BGC}$ is 2.7, indicating that RGCs on average have a higher probability of harboring an LMXB by a factor of 2.7 than BGCs. Although the mean value is consistent with previous reports (e.g., Kundu et al. 2002; Sarazin et al. 2003), we note that galaxy-to-galaxy variations are substantial.

The total number ratio of N(GC LMXBs) to N(field LMXBs is close to 1. We show the run of this ratio as a function of individual galaxy in Figure 7. The most extreme ratios are found in NGC 4374 and NGC 1399. The low ratio of NGC 4374 ($\sim$0.4) appears to be mainly due to the smaller RGC LMXB population, while the higher ratio for NGC 1399 ($\sim$1.8) is due to the small number of field LMXBs in this galaxy. Again we note that galaxy-to-galaxy variations are not negligible (see also § 5).

4. COMPARISON BETWEEN BGC LMXBs, RGC LMXBs, AND FIELD LMXBs

4.1. *GC Luminosity Distribution*

We show the optical luminosity (M_V) distributions of GCs (the whole sample and red/blue GCs separately) in Figure 8. We also plot the luminosity distribution of GCs with LMXBs, for which we use only the LMXBs with net count >20 to minimize the effect of incompleteness, i.e., missing faint X-ray sources. In this plot, we use sources outside of central $20''$ radius.

The amplitude of the observed optical luminosity function of GCs increases as the luminosity decreases and peaks at $M_V \approx -8$. Beyond $M_V \approx -8$ the observed luminosity function drops quickly due to incomplete detection. But note that the true peak of the luminosity function is at $M_V \approx -7.5$ (Richtler 2003). The luminosity function of GCs with LMXBs is different from that of the whole GC sample: the observed peak luminosity is significantly brighter than that of the whole GC sample by $\sim$1.5 mag (or $\sim$4 times brighter), indicating that brighter (bigger) GCs preferentially harbor LMXBs. This is consistent with previous results (e.g., Sarazin et al. 2003). Applying the Kolmogorov-Smirnov (K-S) test to the subsamples used in Figure 8, we find that the probability that GCs with LMXBs are drawn from the same parent population as the whole GC sample is negligible (<1%).

The ratios of the luminosity distribution of GCs (total, blue, and red) with LMXBs and the whole GC samples is shown in Figure 8*b*. Again, there is a clear indication that brighter (bigger)

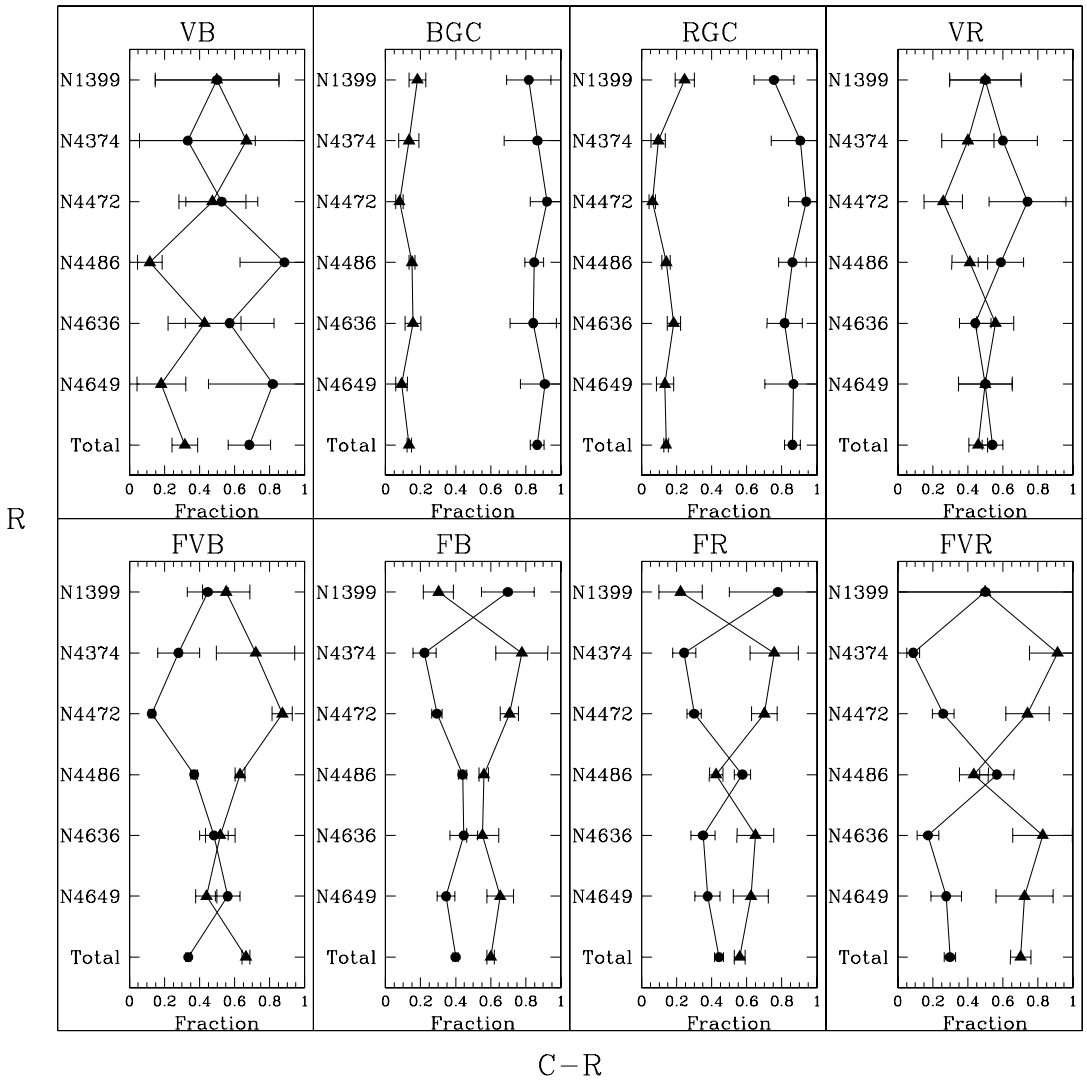

FIG. 5.—Fraction of point sources detected only in ground-based observations (*triangles*) and detected both in ground-based and *HST* WFPC2 observations (*circles*). The panels designated as BGC and RGC represent blue and red GCs, respectively. The CMD region VB (very blue; *top left panel*) represents sources with a bluer color than the color of blue GCs but with the same magnitude range. Similarly, VR (very red; *top right panel*) represents redder sources. FB (faint blue) and FR (faint red) in the bottom panel indicate points sources fainter than blue and red GCs, but with the same colors, while FVB (*bottom left panel*) and FVR (*bottom right panel*) for faint, very blue and faint, very red objects.

GCs preferentially harbor LMXBs. Interestingly, this trend of the optical luminosity dependency is much stronger in RGCs than in BGCs. For example, the fraction of RGCs with LMXB at $M_V = -9.8$ is $\sim$5.5 times higher than that at $M_V = -8.0$, while the fraction of BGCs with LMXBs only changes by a factor of $\sim$2 (see § 5 for more discussion). The K-S test weakly rejects (at the 90% confidence level) the hypothesis that BGCs and RGCs that harbor LMXBs belong to the same population.

4.2. *Radial Distributions of GCs*

Our large sample of sources and the larger optical field of view of the ground-based data allow, for the first time, the studies of the radial variations of GC/LMXB properties, including the optical luminosity of GCs hosting LMXBs, and the X-ray luminosities and colors of GC LMXBs. Previous work, because of the small *HST* field of view, could not extend the study of GC LMXB associations farther than $r > \approx 3'$, where r is the galactocentric radius.

Figure 9 shows the number ratio of GC LMXBs/GCs for different radial regions: (*a*) $R \leq R_{\rm eff}/2$, (*b*) $R_{\rm eff}/2 < R \leq R_{25}/2$, and (*c*) $R_{25}/2 < R \leq R_{25}$, where $R_{\rm eff}$ and R_{25} are from Table 5. We consider only LMXBs with net counts >20. The fact (§ 3.2) that RGCs more preferentially harbor LMXBs than BGCs remains valid in all three radial bins. Also valid is the fact (discussed in § 4.1) that the brighter GCs more preferentially harbor LMXBs. However, it is interesting to note that both RGCs and BGCs located near the galaxy centers have a higher probability of harboring LMXBs compared to the GCs at outskirts. The enhanced probability is most significant for the bright ($M_V < -9$) RGCs, reaching $\sim$20% at the peak in the innermost radial bin. In the outer regions, this probability goes down to $\sim$10%. The difference between the inner region and outer region is statistically significant at the 99% confidence level. For faint GCs, the radial difference is less clear since the number of GCs with LMXBs is small. This radial dependency, which is reported here for the first time, seems to suggest an important mechanism for LMXB formation (see also §§ 4.4 and 5).

4.3. *X-Ray Properties of GC and Field LMXBs*

The X-ray luminosity distributions (normalized to the total number of sources) of LMXBs in different radial regions are

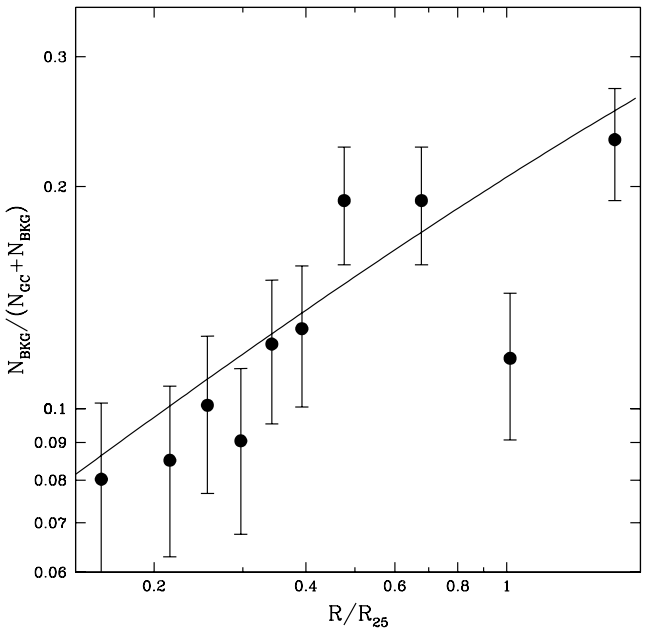

FIG. 6.—Radial profile of the contamination fraction in the ground-based GC sample. The solid line represents the best-fit function $f(r) = 1/(Ar^{-\gamma} + 1)$.

shown in Figure 10. We only consider the X-ray point sources with net counts >20 to minimize incompleteness biases. The X-ray luminosity distributions of different LMXB populations are statistically indistinguishable. The K-S tests for any combination of two samples in the same radial bin suggest that the hypothesis that they are drawn from different populations is excluded at the 95% confidence limit. The only possible exception is the BGC LMXB sample of the central region which appears to peak at higher L_X. However, this difference may be due to the small number (11) of BGC LMXBs.

Figure 11 shows completeness-corrected X-ray luminosity functions (XLFs) of GC LMXBs and field LMXBs, derived by applying the simulation technique as described in Kim & Fabbiano (2004). They are statistically indistinguishable in their shape. Their normalizations are also identical within the error, but this result is not astrophysically meaningful, because of galaxy-to-galaxy variations, as noted in § 3.2 (see also § 5). The only possible difference is observed at the most luminous end ($L_X > 10^{39}$ ergs s^{-1}) of the XLFs, where there are more GC LMXBs than field LMXBs, but with a limited significance ($\sim 1\ \sigma$) due to the small number of very bright LMXBs. We discuss the implications of this result for the presence of black hole (BH) X-ray binaries in GCs in § 5. The individual XLFs of BGC LMXBs and RGC LMXBs are also consistent with each other, except that the XLF of BGC LMXBs is slightly (but within a 1 σ error) flatter. We fit the observed XLFs with both single-power-law and broken-power-law models and find that our results are consistent with those of 14 early-type galaxies studied by Kim & Fabbiano (2004). The best-fit slope for a single power law is 2.1 ± 0.13 for both GC and field LMXBs with χ^2_{red} close to 1. Since the fit with a single power law is already good and a more complex model is not required, the parameters of the broken power law are not well constrained, but our results ($L_{break} = 2 - 10 \times 10^{38}$ ergs s^{-1}; slope = 1.5–2.0 and 2.0–5.0 below and above the break) are consistent with Kim & Fabbiano (2004).

The L_X/L_V luminosity ratios for LMXBs found in GCs are displayed in Figure 12. Again, there is no statistically significant difference in L_X/L_V between any combination of two subsamples. Again the BGC LMXB sample of the central region peaks at the higher L_X/L_V, but this effect is not conclusive because of the large errors. Note that a typical LMXB X-ray luminosity is roughly 10%–30% of the optical luminosity in V band of an entire GC, and a few LMXBs are more luminous than their host GCs ($L_X/L_V > 1$).

To investigate the X-ray spectral properties of different subsamples, we use the X-ray hardness ratio, defined as HR = (H − S)/(H + S), where S and H are net counts in 0.5–2.0 and 2.0–8.0 keV, respectively. We also use X-ray colors as defined in Kim et al. (2004), $C21 = \log(C1/C2)$ and $C32 = \log(C2/C3)$, where $C1$, $C2$, and $C3$ are net counts in 0.3–0.9, 0.9–2.5, and 2.5–8.0 keV, respectively. By definition, as the X-ray spectra become harder, HR increases and X-ray colors decrease. For faint sources with a small number of counts, HR and colors often result in unrealistic values with unreliable errors because of negative net counts in one band and a nonsymmetric Poisson distribution. We apply a Bayesian approach developed by van Dyk et al. (2004), which models the detected counts as a nonhomogeneous Poisson process.

Taking into account the ACIS quantum efficiency degradation, which could change the soft band counts by <20% (Kim et al. 2004), we also convert the counts to what would be obtained at the midpoint within the observation period of our sample.

The mean and standard deviations of each group are listed in Table 10. We find no statistically significant differences in the

TABLE 8
MATCH STATISTICS OF LMXBs AND GCs

		BGC LMXBs		RGC LMXBs		
NAME	$LMXB_{tot}$	G[a]	H[b]	G[a]	H[b]	FIELD LMXBs
$20'' \le R < R_{eff}$						
NGC 1399.....	107	5	5	28	12	29
NGC 4374.....	24	0	3	2	2	13
NGC 4472.....	76	1	5	5	24	33
NGC 4486.....	46	3	4	5	9	20
NGC 4636.....	23	1	2	2	5	13
NGC 4649.....	48	0	1	7	15	21
Total:	324	10	20	49	67	129
$R_{eff} \le R < R_{25}$						
NGC 1399.....	52	10	1	17	0	15
NGC 4374.....	33	3	0	2	0	18
NGC 4472.....	50	6	1	13	1	22
NGC 4486.....	65	9	0	16	6	26
NGC 4636.....	62	5	0	18	0	17
NGC 4649.....	79	10	1	18	2	31
Total:	341	43	3	84	9	129
$R_{25} \le R$						
NGC 1399.....	18	3	0	3	0	8
NGC 4374.....	15	2	0	2	0	3
NGC 4472.....	4	0	0	1	0	2
NGC 4486.....	1	0	0	0	0	0
NGC 4636.....	12	1	0	2	0	8
NGC 4649.....	12	1	0	0	0	9
Total:	62	7	0	8	0	30

[a] Number of sources in optical ground observation only regions.
[b] Number of sources in *HST* observation regions.

TABLE 9
SUMMARY OF MATCH STATISTICS

NAME	N(LMXB) BGC	N(LMXB) RGC	N(LMXB) Field	$N(\mathrm{LMXB_{RGC}})/N(\mathrm{LMXB_{BGC}})$	$N(\mathrm{LMXB_{GC}})/N(\mathrm{LMXB_{field}})$	N(OPT) BGC	N(OPT) RGC	f_{BGC}[a]	f_{RGC}[b]	f_{GC}[c]
NGC 1399.....	21	57	44	2.7 ± 0.7	1.8 ± 0.3	365	434	5.8 ± 1.3	13.1 ± 1.9	9.8 ± 1.2
NGC 4374.....	6	6	31	1.0 ± 0.6	0.4 ± 0.1	298	225	2.0 ± 0.8	2.7 ± 1.1	2.3 ± 0.7
NGC 4472.....	13	43	55	3.3 ± 1.0	1.0 ± 0.2	610	523	2.1 ± 0.6	8.2 ± 1.3	4.9 ± 0.7
NGC 4486.....	16	36	46	2.2 ± 0.7	1.1 ± 0.2	773	740	2.1 ± 0.5	4.9 ± 0.8	3.4 ± 0.5
NGC 4636.....	8	25	30	3.1 ± 1.3	1.1 ± 0.3	453	472	1.8 ± 0.6	5.3 ± 1.1	3.6 ± 0.6
NGC 4649.....	12	42	52	3.5 ± 1.1	1.0 ± 0.2	510	377	2.4 ± 0.7	11.1 ± 1.8	6.1 ± 0.9
Total	76	209	258	2.8 ± 0.4	1.1 ± 0.1	2736	2771	2.8 ± 0.3	7.5 ± 0.5	5.2 ± 0.3

NOTE.—Point sources for $20'' \leq R \leq R_{25}$.
[a] Efficiency of harboring LMXBs, in percent, for blue GCs, defined by $N(\mathrm{LMXB_{BGC}})/N(\mathrm{OPT_{BGC}})$.
[b] Efficiency of harboring LMXBs, in percent, for red GCs, defined by $N(\mathrm{LMXB_{RGC}})/N(\mathrm{OPT_{RGC}})$.
[c] Efficiency of harboring LMXBs, in percent, for all defined by $N(\mathrm{LMXB_{GC}})/N(\mathrm{OPT_{GC}})$.

X-ray HRs and colors of field LMXBs and GC LMXBs and also between RGC LMXBs and BGC LMXBs.

4.4. *Radial Profiles*

We explored spatial differences by comparing the radial profiles of the surface number density of LMXBs and GCs. Because the radial distribution of optical GCs is known to be flatter than that of the optical halo light (e.g., Lee & Kim 2000), it is particularly interesting to test whether the radial profiles of GC LMXBs and field LMXBs follow that of the optical GCs or that of the optical halo light.

We show the combined radial profiles of the surface density of LMXBs, optical GCs, and galaxy halo light (Fig. 13). We fit the radial profile in $0.2 < R/R_{25} < 1.2$. The minimum radius is chosen to minimize missing sources due to highly varying background in both optical and X-ray images, while the maximum radius to minimize the contaminations again in both optical and X-ray sources. The best-fit parameters are summarized in Table 11. As described in § 2.3, we consider the contamination in our GC sample and its radial variation to correct the slope and list them in parentheses in Table 11. On average, the slope gets steeper by ~10%.

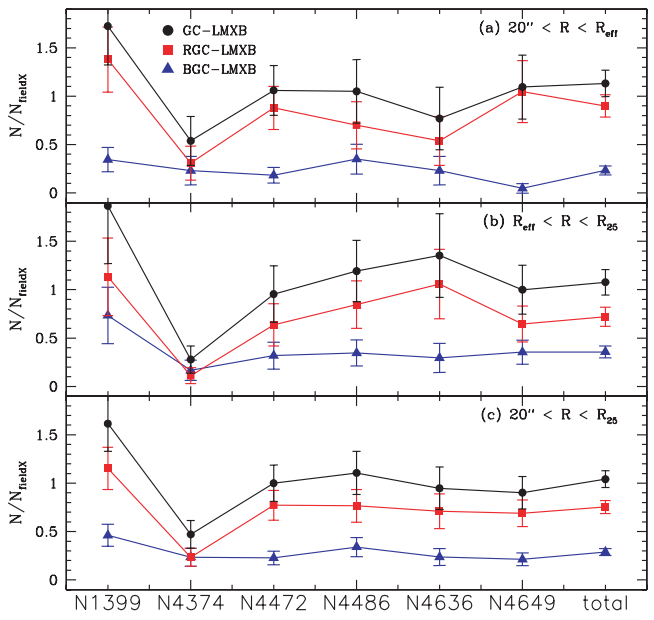

FIG. 7.—Ratio of N(GC LMXBs) to N(field LMXBs) for six galaxies. Filled squares, filled circles, and stars represent the ratios for BGC, RGC, and GC LMXBs, respectively.

As seen in the bottom part of Figure 13, the radial profile of GCs is considerably flatter than that of the optical halo light. This trend is more pronounced in BGCs than in RGCs. This result is consistent with previous optical studies (e.g., Lee & Kim 2000). However, surprisingly, we find that the radial profile of GCs with LMXBs is significantly steeper than that of the optical GC population, but close to that of the halo light (Fig. 13, *top*). The difference of the radial profile slope between the whole GCs and GCs with LMXBs is 1.45, which corresponds to a statistical significance of $>6\,\sigma$ (see Table 11). This result is consistent with our result (§ 4.2) of GCs having a higher chance to harbor LMXBs in the central region and suggests an important clue for the LMXB formation mechanism (see § 5). This trend is also valid for RGCs and BGCs separately. While the radial profile of RGCs (either the entire GC sample or GCs with LMXBs) is steeper than that of BGCs, the radial profile of GCs with LMXBs is still steeper than that of the optical GCs in both BGCs and RGCs samples. It is also interesting to note that the radial profile slope of the field LMXBs is very similar to that of RGC LMXBs, while steeper than, but still consistent with, that of BGC LMXBs.

To make sure that these differences in radial distributions are not a statistical fluke, we performed 1000 simulations by randomly selecting the same number of GCs as observed from the whole GC sample, then fitting the radial profile with the same method used in Figure 13. We find that the probability that the random sample has a steeper slope than the observed is 0.4% (2.8% and 8.7% for BGCs and RGCs separately). To further check for possible contamination by foreground stars and background galaxies, we compared the radial profiles produced by the *HST* data and the ground optical observations separately (Fig. 14). The GC radial profiles produced by ground-based and *HST* data are consistent with each other within a $1\,\sigma$ error for all subpopulations of GCs.

The small deviation of the field LMXB profile from the optical halo light profile is partly due to the contamination by background X-ray sources, although this is unlikely for LMXBs found in GCs. In typical ACIS observations of Virgo elliptical galaxies, X-ray background sources found within $R < R_{25}$ is ~10% (e.g., Kim & Fabbiano 2004). However, a considerable fraction of background X-ray sources (mostly active galactic nuclei) are expected to be among those X-ray sources which are not identified as either GC LMXBs or field LMXBs because typical active galactic nuclei would not be in the same CMD as GCs. We also confirm that as

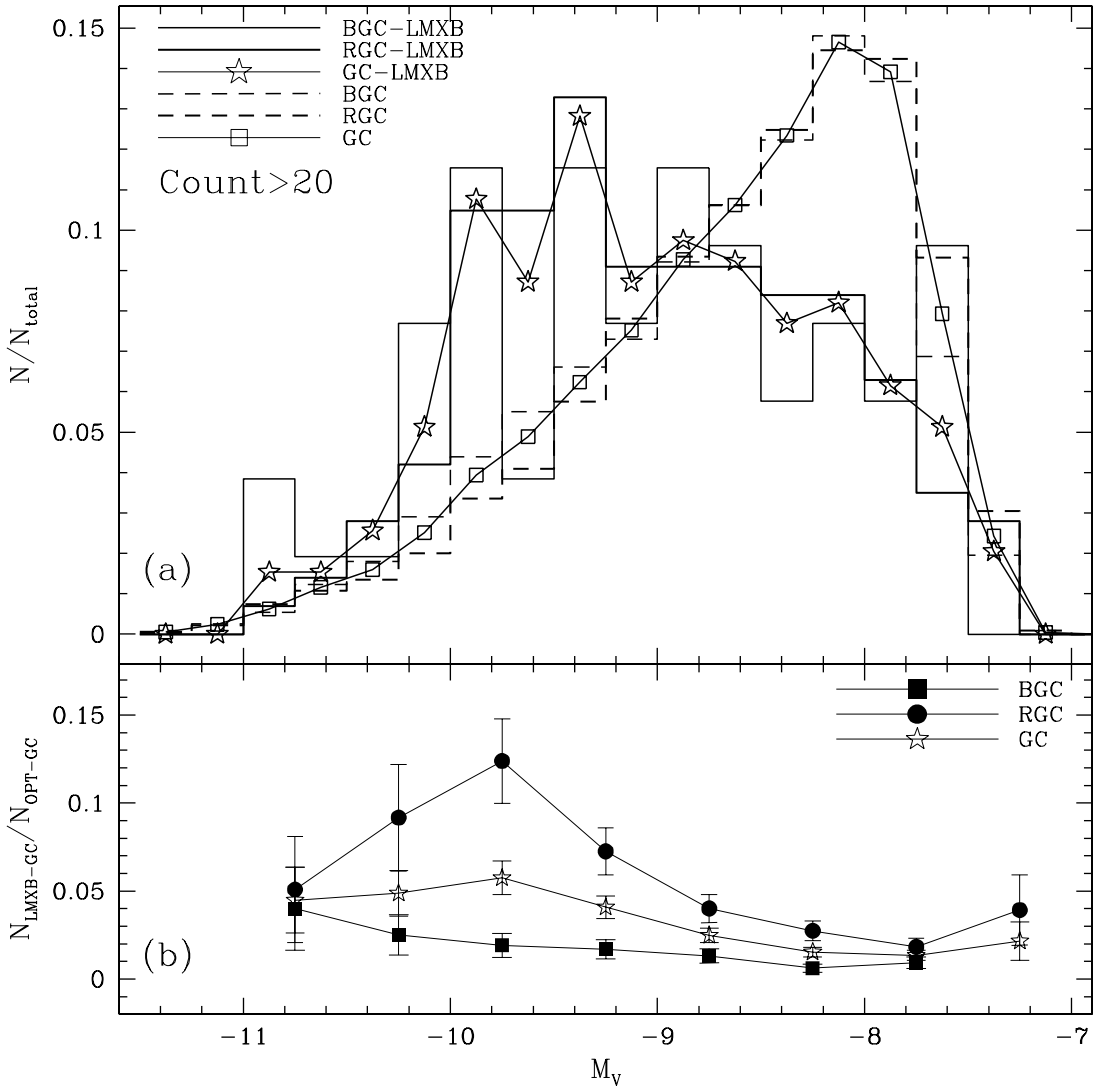

FIG. 8.—(*a*) Optical luminosity function of GCs associated with LMXBs and the entire GC sample. (*b*) Ratio of luminosity functions of GCs with LMXBs to all globular clusters.

expected for the background sources, their radial profile is significantly flatter (by more than 3.3 σ) than those of GC LMXBs and field LMXBs.

5. DISCUSSION

Using *Chandra* and *HST* WFPC2 archival data of six elliptical galaxies, supplemented by deep optical ground-based imaging observations, we identify 6173 GCs and 665 LMXBs within the D_{25} ellipse of these galaxies (§ 2). Applying conservative matching criteria, we find 285 LMXBs coincident with GCs (209 in RGC and 76 in BGC) and 259 LMXBs in the field (§ 3). This is the largest GC + LMXB sample studied so far.

5.1. *Metallicity and LMXB Formation in GCs*

We find that the probability to find LMXBs is on average $\sim$3 times higher for RGCs than BGCs, but with a nonnegligible variation from one galaxy to another (§ 3.2), consistent with previous reports on early-type galaxies (e.g., Kundu et al. 2002; Jordan et al. 2004), and in the Milky Way and M31 (e.g., Grindlay 1993). This result indicates that metal abundance plays a key role in forming LMXBs in globular clusters, as suggested by the above authors.

The physical mechanisms linking the metallicity and the formation and evolution of LMXBs are not well understood. Bellazzini et al. (1995) suggested that the larger stellar size of a metal-rich star can increase the tidal capture rate, making it easier to fill the Roche lobe, and therefore may be responsible for the preferential association of LMXBs with metal-rich RGCs. Instead, Maccarone et al. (2004) showed that the effect of the larger stellar size is not enough to explain the observed difference, and proposed an irradiation induced stellar wind model, where a metal-poor star (in BGC) with a stronger stellar wind evolves more rapidly than a metal-rich star in RGC. This model predicts harder X-ray spectra in BGC LMXBs than RGC LMXBs, because of the extra absorption by accreting materials in BGC LMXBs (their estimated column density $N_{\rm H} \approx 6 \times 10^{21}$ cm^{-2}).

However, when we compare the X-ray spectral hardness/absorption of RGC and BGC sources (§ 4.3), we find no statistically significant differences. Although we cannot rule out a small amount of intrinsic absorption given the statistical uncertainty, we estimate that $N_{\rm H}$ cannot exceed 10^{21} cm^{-2} in both RGCs and BGCs. Therefore, our result does not support the prediction of the stellar wind model. Recently, Ivanova (2005) suggests that the absence of an outer convective zone in the metal-poor

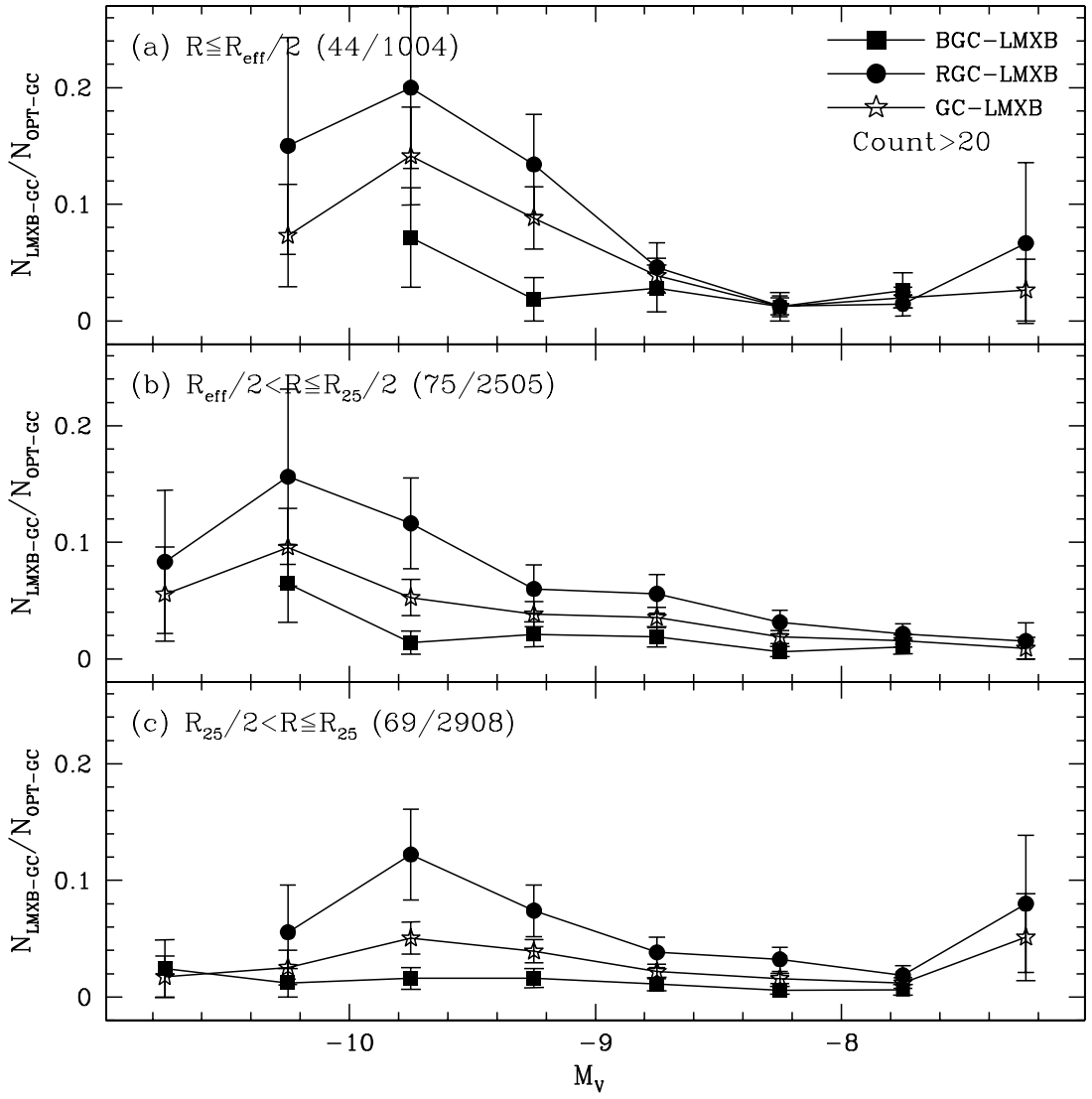

FIG. 9.—Ratio of luminosity functions of GCs with LMXBs and the entire GC for (*a*) the central region, (*b*) the intermediate region, and (*c*) the outer regions. We use the same symbols as in Fig. 8*b*. The numbers in parentheses are the number of GCs with LMXBs and the total number of GCs in each radial region.

main-sequence star may explain the observed trend. Because magnetic breaking, necessary for the orbital decay to form a compact X-ray binary, does not turn on without the outer convective zone, the efficiency to form LMXBs is considerably lower in BGCs than in RGCs. If this scenario is correct, there is no specific reason for different X-ray obscuration and the X-ray spectral properties of LMXBs in RGCs and BGCs would be similar, as indicated in our results. However, no theoretical model, so far, can explain why the fraction of LMXBs in RGCs and BGCs considerably varies from one galaxy to another (from 1.4 to 4.6; § 3.2).

5.2. *Dynamical Effect in GC LMXB Formation*

We have found that the GCs located near the center of galaxies have a higher probability of harboring LMXBs compared to those in the outskirts. This trend is confirmed with a high significance both by the luminosity dependent GC LMXB fractions in different regions (§ 4.2) and by the radial profiles of LMXBs and GCs (§ 4.4). Although a negative radial gradient of the average GC metallicity is known in some elliptical galaxies (e.g., Lee et al. 1998), it can be mostly attributed to the steeper radial profile of metal-rich RGCs, compared to that of metal-poor BGCs (Geisler et al. 1996, as seen in Fig. 13). Therefore, the metallicity gradient for the RGC and BGC individually is not significant (Lee et al. 1998) and cannot explain the observed higher probability of harboring an LMXB near the galactic center than in the outskirts. A secondary mechanism, dependent on the galactocentric distance, must play an important role in the GC LMXB formation, with the metallicity being the primary mechanism as discussed above (Kundu et al. 2002, see also). One possible explanation is that GCs near the galactic center may have a compact core and a higher central density than GCs in the outer regions, as a result of selective GC disruption by the galactic tidal force. This conclusion is also consistent with the recent *HST* study of M31 where the central density of GCs increases toward the center of M31 (Barmby et al. 2002; see also Bellazzini et al. 1995). Therefore, the chance to form LMXBs is expected to increase in GCs near the galaxy center because of a higher rate of either tidal capture or exchange interaction resulting from the higher central stellar density.

Based on the structural parameters of individual GCs determined with the *HST* ACS data of M87, Jordan et al. (2004) showed that the encounter rate (Γ) of GCs with LMXBs is considerably higher than the mean Γ. They formulated a probability of a

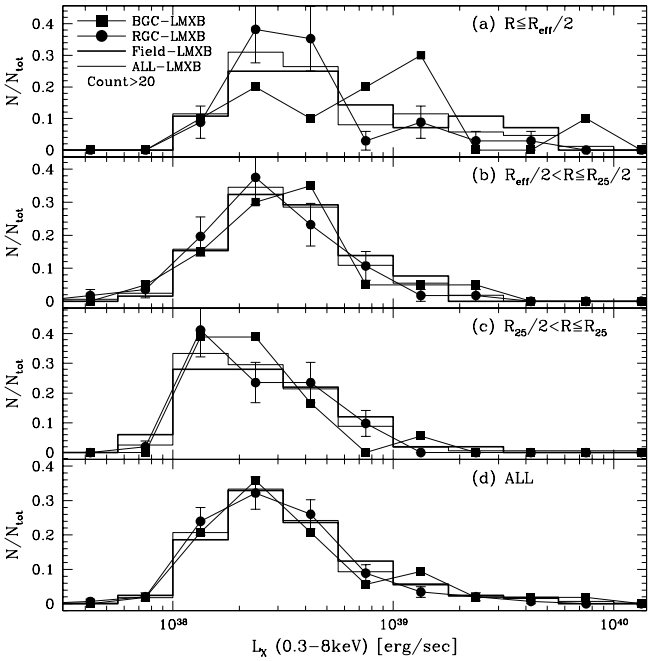

FIG. 10.—Differential luminosity functions of X-ray point sources for (*a*) the central region, (*b*) the intermediate region, (*c*) the outer regions, and (*d*) all radial regions. The filled squares, filled circles, thick solid lines, and thin solid lines represent BGC, RGC, and field LMXBs, and the whole LMXB sample, respectively.

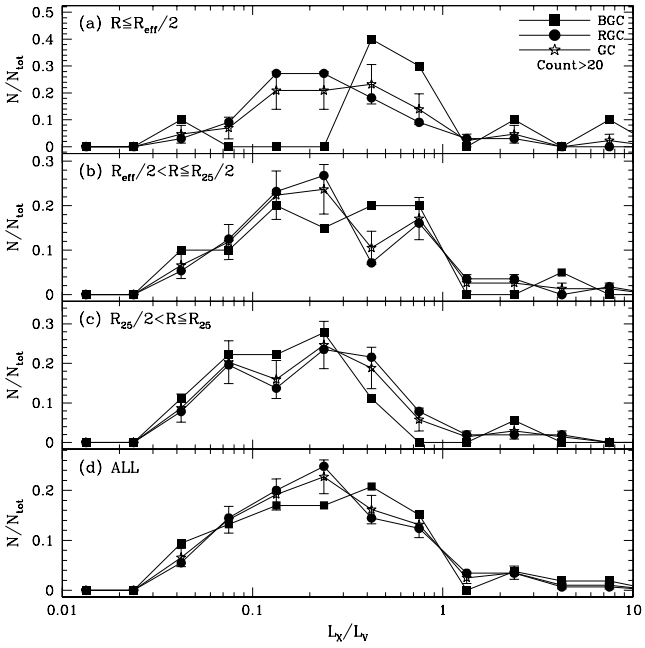

FIG. 12.—Distribution of L_X/L_V for (*a*) the central region, (*b*) the intermediate region, (*c*) the outer regions, and (*d*) all radial regions.

GC hosting an LMXB as a function of Γ and Z. This formulation is consistent with similar results on Galactic GCs by Pooley et al. (2003) and Heinke et al. (2003), and with the higher central density of M31 GCs with LMXBs (Bellazzini et al. 1995). Our results further support that the probability of harboring an LMXB requires a secondary parameter in addition to metallicity.

Based on the correlation between Γ and luminosity, Jordan et al. (2004) also suggested that the luminosity dependency on the fraction of GCs with LMXBs may be a consequence of a more fundamental relation between Γ and luminosity. As reported previously (e.g., Sarazin et al. 2003), we confirm that the more luminous GCs have a higher probability to host LMXBs (§ 4.1). This trend is valid for each RGC and BGC subsample. However, we find that the linearity holds only in RGCs, but not in BGCs. The RGC LMXB fraction increases by a factor of ∼5.5 as M_V increases from −8 mag to −9.8 mag (i.e., brighter by a factor of 5.2). This is consistent with the expected linear increase of the LMXB fraction with increasing luminosity. On the other hand, the BGC LMXB fraction increases only by a factor of ∼2 with the same optical magnitude range. This may indicate a complex relation in metal poor GCs between the cluster luminosity (or mass) and the LMXB fraction, as might be suggested by Ivanova (2005).

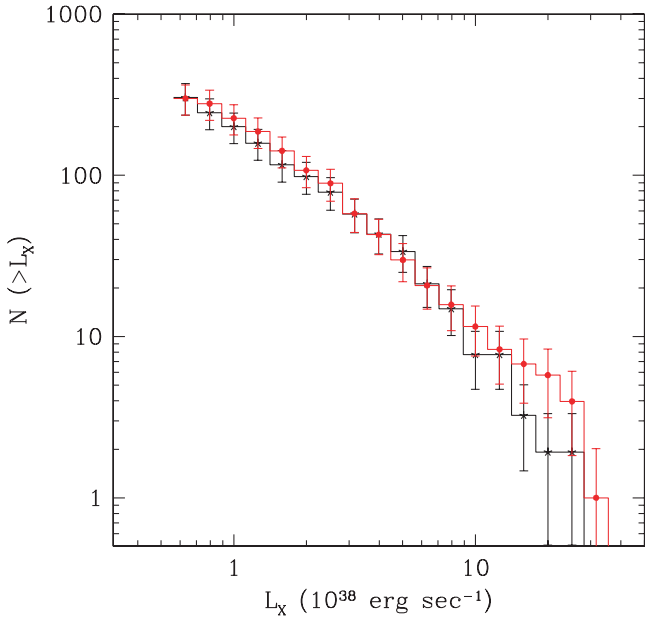

FIG. 11.—XLFs of field LMXBs (*asterisks*) and GC LMXBs (*filled circles*) in six elliptical galaxies.

5.3. *Can Black Hole X-Ray Binaries Form in GCs?*

It is well known that no BH X-ray binary has been found in Galactic GCs (e.g., Grindlay et al. 2001); however, the total number of GC LMXBs in the Milky Way is relatively small. Kalogera

TABLE 10
HARDNESS RATIOS AND X-RAY COLORS OF LMXBS

LXMB Sample	Parameter	$R \le R_{\rm eff}/2$	$R_{\rm eff}/2 < R \le R_{25}/2$	$R_{25}/2 < R \le R_{25}$
BGCs.....	C21	−0.23 ± 0.32	−0.14 ± 0.30	−0.21 ± 0.31
	C32	+0.85 ± 0.51	+0.37 ± 0.30	+0.39 ± 0.28
	HR	−0.81 ± 0.15	−0.62 ± 0.28	−0.73 ± 0.25
RGCs.....	C21	−0.19 ± 0.38	−0.18 ± 0.27	−0.25 ± 0.30
	C32	+0.44 ± 0.35	+0.45 ± 0.33	+0.44 ± 0.31
	HR	−0.65 ± 0.44	−0.68 ± 0.36	−0.64 ± 0.32
GCs	C21	−0.20 ± 0.37	−0.17 ± 0.27	−0.24 ± 0.31
	C32	+0.53 ± 0.42	+0.44 ± 0.32	+0.42 ± 0.30
	HR	−0.68 ± 0.40	−0.67 ± 0.35	−0.67 ± 0.30
Field	C21	−0.14 ± 0.44	−0.18 ± 0.35	−0.20 ± 0.37
	C32	+0.59 ± 0.44	+0.51 ± 0.37	+0.55 ± 0.42
	HR	−0.62 ± 0.56	−0.69 ± 0.34	−0.71 ± 0.35

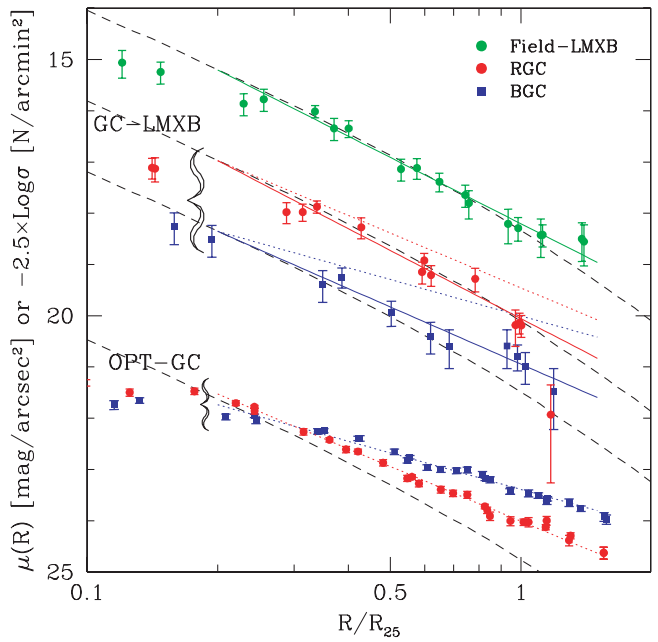

FIG. 13.—Radial profiles of point sources and the combined galaxy light. The radial profiles for optical GCs in the bottom part and LMXBs in the top part are scaled to be compared directly to that of the optical halo light. The curved dashed lines represents the scaled galaxy halo light after shifting upward and downward for easy comparison with other profiles. The different symbols represent BGC (*blue squares*), RGC (*red circles*), and field LMXBs (*green circles*). The red/blue solid line shows best-fit for LMXBs in RGCs/BGCs, while the red/blue dotted line for optical RGCs/BGCs.

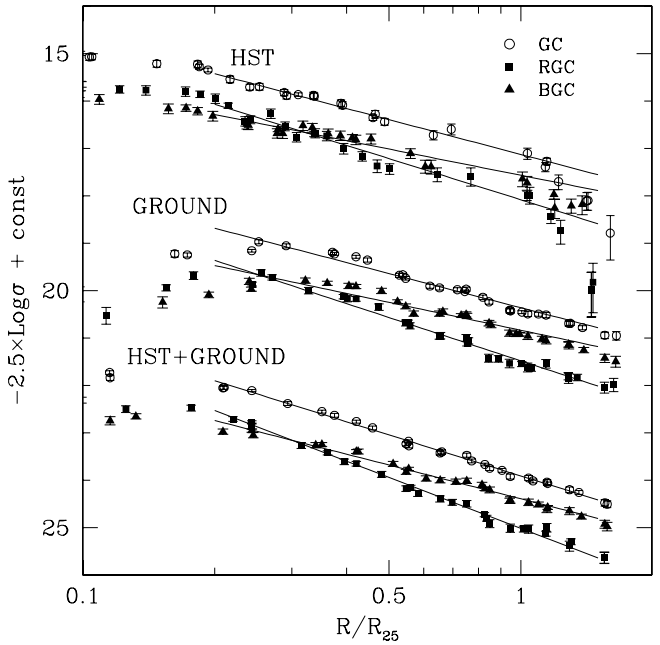

FIG. 14.—Radial profiles of optical globular cluster candidates for *HST* observations, ground-based observations, and a combination of ground-based and *HST* observations.

et al. (2004) showed that the duty cycle for a BH binary formed in the center of a dense cluster by an exchange interaction is extremely low. For early-type galaxies, mixed results have been reported. Sarazin et al. (2003) reported a weak tendency for bright LMXBs to avoid GCs and Minniti et al. (2004) reported that no bright GC LMXB (i.e., BH candidates) is identified in NGC 5128. On the other hand, a number of luminous GC LMXBs are found in N1399 (Angelini et al. 2001) and M87 (Jordan et al. 2004). Angelini et al. (2001) have even claimed that GC LMXBs are on average more luminous than the field LMXBs. We found with high statistical confidence (§ 4.3) that the XLFs of GC LMXBs and field LMXBs are statistically consistent, indicating that luminous LMXBs are equally found in GCs and in the field. More specifically, there are 26 GC LMXBs and 27 field LMXBs with $L_X > 5 \times 10^{38}$ ergs s^{-1}. We note that $L_X = 5 \times 10^{38}$ ergs s^{-1} corresponds to the break luminosity of the LMXB XLF where NS and BH X-ray binaries are likely separated, as identified by Kim & Fabbiano (2004). More conservatively, if we consider $L_X > 10^{39}$ ergs s^{-1}, there are still eight GC LMXBs and three field LMXBs.

Therefore, our results do not support the hypothesis that a GC cannot harbor a BH X-ray binary.

TABLE 11

LINEAR LEAST-SQUARED FITTING OF RADIAL PROFILES

Sample	Slope	σ	Sample	Slope	σ
BGCs.....	2.36 ± 0.05	0.08	BGC LMXBs.....	3.71 ± 0.54	0.18
	(2.73 ± 0.05)	(0.09)		(4.16 ± 0.59)	(0.19)
RGCs.....	3.55 ± 0.05	0.08	RGC LMXBs.....	4.41 ± 0.30	0.49
	(3.93 ± 0.05)	(0.06)		(4.81 ± 0.32)	(0.18)
GCs	2.87 ± 0.03	0.05	GC LMXBs.....	4.32 ± 0.23	0.18
	(3.24 ± 0.04)	(0.06)		(4.69 ± 0.25)	(0.14)
Halos	4.60 ± 0.04	0.05	Field LMXBs.....	4.31 ± 0.26	0.13

NOTE.—Numbers in parentheses are fitting result for the background-corrected GC sample based on Figs. 5 and 6.

5.4. *Are Field LMXBs Formed in the Field or in GCs?*

We find on average an equal number of LMXBs in GCs and in the field, although with a nonnegligible galaxy-to-galaxy variation. One of the key questions for understanding LMXB formation is whether GCs are the only birth place for all LMXBs. In this scenario, field LMXBs were originally formed in GCs and were then ejected from the parent GC or left alone in the field as the GC was disrupted (e.g., Bildsten & Deloye 2004). Utilizing the fact that the radial profile of GCs is flatter than that of the galactic halo light (e.g., Lee et al. 1998), we tested this hypothesis by determining whether the radial profile of field LMXBs follows that of GCs or that of the halo light. We found (§ 4.4) that regardless of their association with GCs, LMXBs are distributed like the optical halo light, not the GCs. The close agreement between the radial distributions of the optical light and LMXBs has also been reported in NGC 1316 (Kim & Fabbiano 2003), NGC 1332 (Humphrey & Buote 2004), and NGC 4486 (Jordan et al. 2004). This seems to suggest a rather complex connection, depending on various factors operating in the LMXB formation in GCs and its subsequent evolution (see § 5.2). Because of the similar radial distribution between GC LMXBs and field LMXBs, we can neither prove nor reject the hypothesis whether field LMXBs were originally formed in the GC.

If field LMXBs were ejected from GCs, they may still be in the neighborhood of the parent cluster. We therefore searched for a nearby GC, which could have been the previous host of the current field LMXB, and compared the results with the expectation from the mean space density of GCs. First, we find that the mean angular distance of the nearest GC from the field LMXBs is 5″–10″. This is compatible with the expected mean random separation,

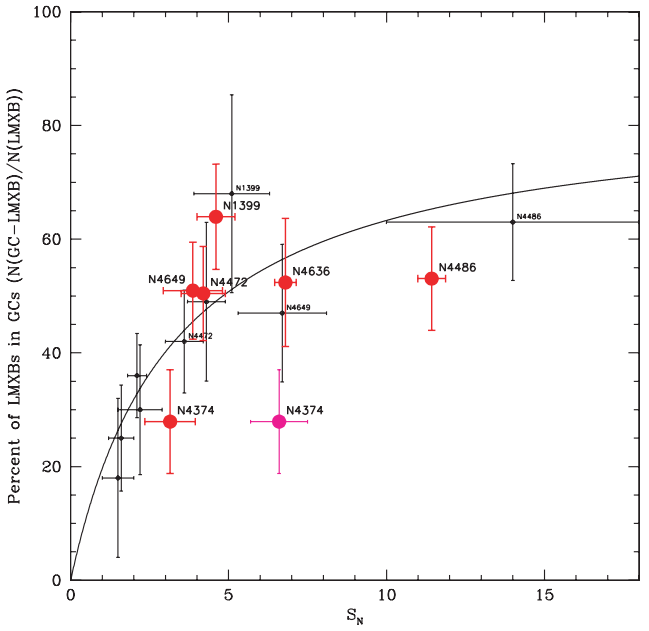

FIG. 15.—Fraction of the LMXB population found in GCs plotted against the GC-specific frequency, S_N. The data for galaxies in the present study are shown with red circles while the data from Juett (2005) with small open circles. Two values of S_N for NGC 4374 are from Gómez & Richtler (2004) (*red*) and Kissler-Patig (1997) (*magenta*).

based on the space density of GCs ($\sim 8''$), indicating that there is no preference to find a potential host GC near a field LMXB. Second, we measure the GC surface density near the field LMXBs. Again, the estimated density is comparable with that expected from the GC space density ($\sim$18 GCs arcmin^{-2}).

Based on simple relations of f(GC LMXB) and L_X(LMXB) against the GC specific frequency (S_N), Juett (2005) and Irwin (2005) suggested that a considerable fraction of field LMXBs were indeed formed in the field. Although this suggestion is intriguing, reality may be more complex. Their relations may test the hypothesis of field LMXBs ejected from the parent GCs, but cannot work if the parent GCs were disrupted, because the current S_N would not include GCs disrupted in the past. Furthermore, because S_N is usually determined from large scale observation (compared to the *HST* field of view), it is important to determine LMXB properties in spatial region comparable to that used to decide S_N. However, the previous studies are mostly limited to the *HST* WFPC2 field of view. If we plot our data of Table 9 in the same figure of Juett (2005), the relation appears to be less convincing (Fig. 15). Most galaxies (four of six) have almost constant f(GC LMXB) (50% $\pm$ 5%), but with a wide range of $S_N = 4-12$ (from Dirsch et al. 2005; Kissler-Patig 1997; Rhode & Zepf 2001; Forbes et al. 2004). The remaining two galaxies are also outliers. NGC 4374 has the smallest GC LMXB fraction (30%) in our sample, but with a rather modest S_N (3.2 [Gómez & Richtler 2004; Harris 1991] or 6.6 [Kissler-Patig 1997]). NGC 1399 has the highest GC LMXB fraction (65%) in our sample, but S_N is only 4.6 (Dirsch et al. 2003). Therefore, the proposed relationship with S_N does not appear to be straightforward. The situation could be even more complex, for example, because of different merger histories (e.g., Schweitzer 2003) and different degrees of environment-dependent GC stripping (Bekki et al. 2003), which would add significant galaxy-to-galaxy variations. In particular, we note that three galaxies with the lowest GC LMXB fraction (NGC 1553, NGC 3115, and NGC 1332) are all S0 galaxies.

Although we have mitigated the mismatch between sampling regions of S_N and f(GC LMXB) by extending our analysis to radii larger than the *HST* WFPC2 field of view, the problem still remains as S_N is often determined at the even larger regions and moreover it varies as a function of radius. It is therefore important to determine S_N in the same region as the GC LMXB fractions.

6. CONCLUSIONS

1. In our sample of six elliptical galaxies, we find 285 LMXBs matched with GCs (209 in RGCs and 76 in BGCs) and 259 LMXBs in the field. This is the largest sample studied so far. We estimate that the systematic error in LMXB-GC associations due to the source contamination and false matches is 5%–10%.

2. We confirm that on average the fraction of RGCs with LMXBs is 3 times higher that of BGCs with large variations from one galaxy to another, indicating that metallicity is an important factor in GC LMXB formation (Kundu et al. 2002; Jordan et al. 2004). We find that the average X-ray spectra of RGC and BGC LMXBs are statistically identical, in disagreement with the prediction of the stellar wind model (Maccarone et al. 2004), but consistent with the explanation of the lack of outer convective zone in BGCs (Ivanova 2005). We also find that while the brighter (and bigger) GCs have a higher probability of hosting LMXBs as suggested by Sarazin et al. (2003), this linear dependency on the optical luminosity only holds in RGCs, possibly implying a complex formation scenario in BGCs (e.g., Ivanova 2005).

3. Both RGCs and BGCs located near the galaxy center have a higher probability of harboring LMXBs than GCs at the outer radii. The same trend is also confirmed by the steeper radial profile of GC LMXBs (for both RGCs and BGCs), when compared to that of the whole GC sample. This suggests there must be another parameter (in addition to metallicity) for LMXB formation in GCs, which critically depends on the galactocentric distance. One possibility is a variable encounter rate, depending on the galactocentric distance, as suggested by Jordan et al. (2004).

4. We find no statistically significant difference in the X-ray properties (shape of X-ray luminosity function, L_X/L_V distribution, X-ray spectra) among RGC, BGC, and field LMXBs. In particular, there is no observational preference to host or avoid BH X-ray binaries in GCs.

5. We find on average an equal number of LMXBs in GCs and in the field. We have tested the hypothesis that field LMXBs were once formed in GCs, by comparing radial profiles of GC LMXBs and field LMXBs and by searching for possible parent GCs near field LMXBs. We find that LMXBs, regardless of their association with GCs, do not follow the radial distribution of GCs, but more closely follow that of the optical halo light. The average distance and density of GCs near the field LMXBs are consistent with the expectation from the mean GC space density. Therefore, we could neither prove nor reject this hypothesis.

This work was supported by *Chandra* GO program GO3-4109X and *Chandra* archival research grant AR7-0001X. D. W. K. and G. F. acknowledge support through NASA contract NAS8-39073 (CXC). M. G. L. was supported in part by grant R01-2004-000-10490-0 from the Basic Research Program of the Korea Science and Engineering Foundation.

REFERENCES

Angelini, L., Loewenstein, M., & Mushotzky, R. F. 2001, ApJ, 557, L35
Barmby, P., Holland, S., & Huchra, J. P. 2002, AJ, 123, 1937
Bekki, F., Forbes, D. A., Beasley, M. A., & Couch, W. J. 2003, MNRAS, 344, 1334
Bellazzini, M., et al. 1995, ApJ, 439, 687
Bildsten, L., & Deloye, C. J. 2004, ApJ, 607, L119
Casertano, S., et al. 2000, AJ, 120, 2747
Chandra X-Ray Center 2004, *Chandra* Proposer's Observatory Guide (ver. 7.0; Cambridge: CXC)
de Vaucouleurs, G., de Vaucouleurs, A., Corwin, H., G., Jr., Buta, R., J., Paturel, G., & Fouqué, P. 1991, Third Reference Catalogue of Bright Galaxies (New York: Springer)
Dirsch, B., Richtler, T., Geisler, D., Forte, J. C., Bassino, L. P., & Gieren, W., P. 2003, AJ, 125, 1908
Dirsch, B., Schuberth, Y., & Richtler, T. 2005, A&A, 433, 43
Dolphin, A. E. 2000, PASP, 112, 1383
Forbes, D. A., et al. 2004, MNRAS, 355, 608
Forte, J. C., Faifer, F., & Geisler, D. 2005, MNRAS, 357, 56
Geisler, D. 1996, AJ, 111, 480
Geisler, D., Lee, M. G., & Kim, E. 1996, AJ, 111, 1529
Gómez, M., & Richtler, T. 2004, A&A, 415, 499
Grindlay, J. 1993, in ASP Conf. Ser. 48. ed. G. H. Smith & J. P. Brodie (San Francisco: ASP), 156
Grindlay, J., Heinke, C. O., Edmonds, P. D., Murray, S. S., & Cool, A. M. 2001, ApJ, 563, L53
Grindlay, J., & Hertz, P. 1985, in Cataclysmic Variables and Low-Mass X-Ray Binaries, ed. D. Lamb & J. Patterson (Dordrecht: Reidel), 79
Harris, W. E. 1991, ARA&A, 29, 543
Heinke, C. O., Grindlay, J. E., Edmonds, P. D., Lyoyd, D. A., Murray, S. S., Cohn, H. N., & Lugger, P. M. 2003, ApJ, 598, 516
Humphrey, P. J., & Buote, D. A. 2004, ApJ, 612, 848
Irwin, J. 2005, ApJ, 631, 511
Ivanova, N. 2005, ApJ, 636, 979
Jedrzejewski, R., I. 1987, MNRAS, 226, 747
Jordan, A., et al. 2004, ApJ, 613, 279
Juett, A., M. 2005, ApJ, 621, L25
Kalogera, V., King, A. R., & Rasio, F. A. 2004, ApJ, 601, L171
Kim, D.-W., & Fabbiano, G. 2003, ApJ, 586, 826
———. 2004, ApJ, 613, 933
Kim, D.-W., et al. 2004, ApJ, 600, 59
Kim, E., Lee, M. G., & Geisler, D. 2000, MNRAS, 314, 307
Kim, M., Kim, E., Lee, M. G., Sarajedini, A., & Geisler, D. 2002, AJ, 123, 244
Kim, M., et al. 2006, ApJS, in press
Kissler-Patig, M. 1997, A&A, 319, 83
———. 2000, Rev. Mex. AA, 13, 13
Kundu, A., Maccarone, T. J., & Zepf, S. E. 2002, ApJ, 574, L5
Kundu, A., Whitmore, B. C., Sparks, W. B., Macchetto, F. D., Zepf, S., & Ashman, K. M. 1999, ApJ, 513, 733
Larsen, S. S., Brodie, J. P., Huchra, J. P., Forbes, D. A., & Grillmair, C. J. 2001, AJ, 121, 2974
Lee, M. G., & Kim, E. 2000, AJ, 120, 260
Lee, M. G., Kim, E., & Geisler, D. 1998, AJ, 115, 947
Maccarone, T. J., Kundu, A., & Zepf, S. E. 2004, ApJ, 606, 430
Minniti, D., Rejkuba, M., Funes, S. J., Josi, G., & Akiyama, S. 2004, ApJ, 600, 716
Monet, D., et al. 2003, USNO-B1.0, A Catalog of Astrometric Standards (Flagstaff: Naval Obs.)
Pooley, D., et al. 2003, ApJ, 591, L131
Rhode, K., & Zepf, S. 2001, AJ, 121, 210
Richtler, T. 2003, in Stellar Candles for the Extragalactic Distance Scale, ed. D. Alloin & W. Gieren (Berlin: Springer), 281
Sarazin, C. L., Irwin, J. A., & Bregman, J. N. 2001, ApJ, 556, 533
Sarazin, C. L., et al. 2003, ApJ, 595, 743
Schweitzer, F. 2003, in ASP Conf. Ser. 296, New Horizons in Globular Cluster Astronomy, ed. Piotto, G., et al. (San Francisco: ASP), 467
Stetson, P. B. 1987, PASP, 99, 191
van Dyk, D. A., Park, T., Kashyap, V. L., & Zezas, A. 2004, AAS HEAD Meeting, 8, 1627
Verbunt, F., & Lewin, W. 2006, in Compact Stellar X-Ray Sources, ed. W. Lewin & M. van der Klis (Cambridge: Cambridge Univ Press), 341
Weisskopf, M. C., Tananbaum, H. D., Van Speybroeck, L. P., & O'Dell, S. L. 2000, Proc. SPIE, 4012, 2
White, R. E., III., Sarazin, C. L., & Kulkarni, S. R. 2002, ApJ, 571, L23
Williams, R. E., et al. 1996, AJ, 112, 1335